Application of an Eulerian–Lagrangian–Agent method (ELAM) to rank alternative designs of a juvenile fish passage facility

L. J. Weber, R. A. Goodwin, S. Li, J. M. Nestler and J. J. Anderson

ABSTRACT

The Eulerian–Lagrangian–Agent method (ELAM) couples three modelling approaches into a single, integrated simulation environment: (i) Eulerian descriptions, (ii) Lagrangian formulations, and (iii) agent reference frameworks. ELAMS are particularly effective at decoding and simulating the motion dynamics of individual aquatic organisms, using the output of high fidelity computational fluid dynamics (CFD) models to represent complex flow fields. Here we describe the application of an ELAM to design a juvenile fish passage facility at Wanapum Dam on the Columbia River in the United States. This application is composed of three parts: (1) an agent-based model, that simulates the movement decisions made by individual fish, (2) an Eulerian CFD model that solves the 3D Reynolds-averaged Navier–Stokes (RANS) equations with a standard $k-\varepsilon$ turbulence model with wall functions using a multi-block structured mesh, and (3) a Lagrangian particle-tracker used to interpolate information from the Eulerian mesh to point locations needed by the agent model and to track the trajectory of each virtual fish in three dimensions. We discuss aspects of the computational mesh topology and other CFD modeling topics important to this and future applications of the ELAM model for juvenille salmon, the Numerical Fish Surrogate. The good match between forecasted (virtual) and measured (observed) fish passage proportions demonstrates the value-added benefit of using agent-based models (i.e. the Numerical Fish Surrogate model) as part of common engineering practice for fish passage design and, more fundamentally, to simulate complex ecological processes.

Key words | computational fluid dynamics, computer-based simulation, ecohydraulics, ecological modeling, environmental hydroinformatics, fish modeling, fish passage, individual-based modeling

L. J. Weber (corresponding author)
IIHR Hydroscience & Engineering,
College of Engineering,
University of Iowa,
Iowa City, IA 52242-1585, USA
Tel:+1 319 335 5597;
E-mail: *larry-weber@uiowa.edu*

R. A. Goodwin
Research Environmental Engineer,
Environmental Laboratory,
US Army Engineer Research & Development Center, CENWP-EC-HD, 333 SW 1st Ave,
PO Box 2946, Portland, OR 97208, USA
Tel:+1 503 808 4872;
E-mail: *rag12@cornell.edu*

S. Li
IIHR Hydroscience & Engineering, College of Engineering, University of Iowa,
Iowa City, IA 52242-1585, USA
Tel:+1 319 335 6061;
E-mail: *songheng-li@uiowa.edu*

J. M. Nestler
Environmental Modeling & System-Wide Assessment Center (CEERD-IV-Z),
US Army Engineer Research & Development Center, 3909 Halls Ferry Rd,
Vicksburg, MS 39180-6199, USA
Tel:+1 601 634 2720;
E-mail: *john.m.nestler@erdc.usace.army.mil*

J. J. Anderson
School of Aquatic & Fishery Sciences,
University of Washington,
1325 4th Ave., Suite 1820, Seattle, WA 98101, USA
Tel:+1 206 543 4772;
E-mail: *jim@cbr.washington.edu*

NOTATION

The following symbols are used in this paper:

a_i	the ith component of acceleration
a_D	acceleration in velocity direction ($a_D = U_i a_i / V_M$)
$A, A_f^i, A_{\rightarrow}$	face area, components of face area vector, and face area vector
A_0, A_1, A_2, A_3	environmental stimulus agents
B_0, B_1, B_2, B_3	movement behavior response to agents
$C_\mu, C_{\varepsilon 1}, C_{\varepsilon 2}$	coefficients in turbulence $k-\varepsilon$ model
g	gravity acceleration
G	generation of turbulence kinetic energy
k	turbulence kinetic energy
k_1, k_2, k_3	thresholds in the perceived change of stimulus intensity indicating presence of agent
P	piezometric pressure ($= p' + \rho g z$, p' =hydrostatic pressure)

doi: 10.2166/hydro.2006.006

S_1	distortion metric (total hydraulic strain) using simplified method
S_2	distortion metric (total hydraulic strain) using the Frobenius norm
t	time
T_i	turbulence intensity ($= \sqrt{2k/3}/U$)
U, U_i	mean velocity and velocity components
u_i	fluctuating velocity components ($i = 1, 2, 3$)
$-\rho\overline{u_i u_j}$	Reynolds stresses
V_{CV}	the volume of the computational cell
V_M	velocity magnitude
x_i	Cartesian coordinates ($i = 1, 2, 3$)
z	vertical distance from a reference point
$\alpha_{\max}$, $\alpha_{\min}$, α_e	maximum, minimum, and equilateral angle
δ_{ij}	Kronecker symbol ($\delta_{ij} = 1$ when $i = j$, $\delta_{ij} = 0$ when $i \neq j$)
ε	turbulence dissipation rate
μ	dynamic viscosity
μ_t	turbulence viscosity ($= \rho\nu_t$)
ν_t	eddy viscosity
ρ	water density
σ_k, σ_ε	coefficients in turbulence k–ε model

INTRODUCTION

Mitigating the decline of native salmon stocks is an important environmental and societal issue in the Columbia and Snake River basin of the Pacific Northwest, USA. One of several possible mitigation actions is to increase the proportion of downstream outmigrating juvenile salmon (migrants) that pass hydropower dams without injury on their journey to the ocean. Migrants passing through turbines can be subjected to 5–30% mortality (Neitzel *et al.* 2004). Therefore, research efforts over several decades have been mostly devoted to diverting migrants over spillways and through bypass systems so that passage through the powerhouse turbines can be reduced. However, researchers have only been able to incorporate anecdotal or qualitative fish behavior into consideration when developing bypass systems (Popper & Carlson 1998). Consequently, early bypass systems often achieved only limited and variable success (Coutant & Whitney 2000) at considerable cost (Harden 2003) because migrants could either not locate the opening to the bypass or rejected the opening once they were within its hydraulic influence.

Many potential structural and operational solutions to improve passage efficiency are outside measured natural conditions or previous experience of the designers and, therefore, require numerical modeling tools (Booker *et al.* 2004) for design assessment. A quantitative tool that can be used to help interpret observed data or to forecast migrant movement behavior and response to alternative structural and operational configurations would be of considerable utility both because of the value of salmon and because of the cost of bypass systems. We decided to use an individual based modeling approach to decode how migrants react to features in flow fields and, therefore, understand the success or failure of past bypass systems. An individual approach seems appropriate, as the perception and response of an individual migrant to its environment is undoubtedly complex (Steel *et al.* 2001) because, while individual movements can be translated into an understanding of population dynamics, the converse is generally not possible (Turchin 1997). Hydroinformatics tools needed to understand and model individual migrant movement response to environmental cues are now becoming available (Mynett 2002; Mynett *et al.* 2004). Advances in telemetry (e.g., Steig 1999; Gerolotto *et al.* 1999; Lucas & Baras 2000) can provide high-resolution 3D tracks of individual movements that can be used to formulate and calibrate virtual fish. Computational fluid dynamics (CFD) models can now describe hydrodynamic patterns at scales meaningful to fish, and laboratory studies have recently defined sensory abilities of fish to distinguish elements of hydrodynamic fields (e.g. Coombs *et al.* 2001; Kröther *et al.* 2002).

We describe below an application of an integrated mathematical method that couples (1) an Eulerian framework governing the physical and hydrodynamic domain of a hydropower dam forebay, (2) a Lagrangian framework governing the sensory perception and movement trajectories of individual fish, and (3) an Agent-based framework governing the cognitive domain and behavioral decisions of individual fish. The resulting Eulerian–Lagrangian–Agent Method (ELAM) decision-support tool for migrants is called the Numerical Fish Surrogate (NFS) model (Goodwin *et al.* 2006). We describe hereafter an application of NFS as one of several project evaluation tools to rank alternative bypass

designs for Wanapum Dam. We focus here on hydro (CFD) and informatics issues associated with applying NFS. Our application demonstrates that behavioral stimuli and responses can be incorporated into common engineering practice for fish protection as suggested by Popper & Carlson (1998). Accuracy of the Numerical Fish Surrogate is assessed by comparing the model's ability to rank existing bypass systems versus measured performance (Goodwin *et al.* 2006).

WHY EULERIAN, LAGRANGIAN, AND AGENT FRAMEWORKS ARE ALL NEEDED

Processes in the physical sciences are generally analyzed using one or a combination of three approaches: Eulerian, Lagrangian, and Agent-based (object-orientated) (Nestler *et al.* in press). From a fluid mechanics perspective, the Eulerian approach efficiently describes fluid motion and its associated properties (e.g. the acceleration field a) in terms of mass/momentum/energy fluxes at numerous fixed locations (e.g. nodes in a mesh with x, y, z locators) as a function of time t (viz. $a = a(x, y, z, t)$). The Lagrangian approach tracks and describes individual fluid "particles" as they move within the physical domain as a function of time. Using numerous particles can provide information on a flow behaviour at many locations in the system as a function of time, but the fluid property would not be known as a function of position unless the location of each particle were known as a function of time. In fluid mechanics, the Eulerian approach is usually preferred to describe the fluid flow, although there are situations where a Lagrangian approach is more convenient (e.g. in the case of local outfalls into ambient stagnant fluids). Measuring the rate at which fish pass a certain location (fish per second) corresponds to the Eulerian approach, i.e. a "flux" of fish at a given location as a function of time, but the identity of individual fish is not maintained. Following the motion of individual fish with transmitters corresponds to a Lagrangian approach, i.e. the "position" of a fish is given as a function of time. An agent-based approach is required to analyze and simulate behavior, learning, and memory of individuals since neither the Eulerian nor Lagrangian approaches have such capabilities.

A New Paradigm – Eulerian–Lagrangian–Agent Methods (ELAMs)

The Eulerian–Lagrangian–Agent Method (ELAM) can mechanistically decode (interpret) and forecast 3D movement patterns of individual fish responding to modeled or measured stimuli. The ELAM framework is well suited for describing large-scale patterns in hydrodynamics and water quality as well as for zooming in on much smaller scales at which individual fish make their movement decisions. This ability of ELAM models to simultaneously handle dynamics at multiple scales allows them to 7realistically represent fish movements within aquatic systems (Goodwin *et al.* 2006) and can be applied to other problems where processes over a wide range in scale must be accommodated.

Hypothesis of migrant movement behavior

The importance of a particular type of stimulus (e.g. odor, predator, prey, or hydrodynamics) to a fish, and therefore its likely response, varies with the context of the stimulus (Kim & Wardle 2005). Near dams, the response of fish to hydrodynamics frequently overrides or supersedes their responses to other stimuli (Popper & Carlson 1998). Through natural selection riverine fish have evolved behaviors in response to hydrodynamic stimuli (Kalmijn 2000). Aquatic environments are rich in acoustic and hydrodynamic signals (Rogers & Cox 1988) because any object that moves relative to a fluid generates a disturbance field (Montgomery *et al.* 1995). Fish can detect flow strength and direction (Montgomery *et al.* 2000; Voigt *et al.* 2000); whole body acceleration (Kalmijn 1989); near-instantaneous spatial velocity gradients (Hudspeth 1989) describing normal strain, shearing strain, and rotation (the mechanisms of flow field distortion); and pressure (Coutant 2001). Although what a fish perceives is undoubtedly complex, we believe that their response to features in flow fields near dams can be understood by considering basic principles of (i) hydrogeomorphology, (ii) the terms of the Navier–Stokes equations of fluid motion, and (iii) the structure and capabilities of the fish sensory system. We term the resulting synthesis as the strain–velocity–pressure (SVP) hypothesis (Goodwin 2004).

Quantifying flow field distortion using "total hydraulic strain"

In our modeling system, fish move through the forebay of a large hydropower dam and are assumed to respond only to hydrodynamic cues generated by forebay structures without visual cues from or tactile contact with solid structures. General fluid motion can be described as the sum of four mechanisms: (1) linear translation, (2) linear deformation, (3) rotation, and (4) angular deformation. Spatial velocity variation induces (2) linear deformation, (3) rotation, and (4) angular deformation mechanisms. If we define distortion as the sum of deformation and rotation mechanisms, i.e. all fluid motion mechanisms other than simple linear translation, the spatial velocity gradient tensor embodies all of the information needed to define a "total distortion" metric. It seems plausible that fish can detect each spatial velocity gradient separately and at a near instantaneous interval because subcutaneous canals of the mechanosensory lateral line system are oriented differently over the body of the fish. Popper and Carlson (1998) point to studies in Suckling and Suckling (1964) and Anderson and Enger (1968) indicating fish detect water particle movements of less than 0.5 μm. However, with little-to-no guidance on how, or if, fish may assemble and respond to the instantaneous spatial velocity gradients describing flow field distortion, we assemble them into a hypothetical scalar total distortion metric, S_1, using the simplest way possible by summing the absolute values of each spatial velocity gradient:

$$S_1 = \Sigma|\partial u_i/\partial x_j| = |\partial u/\partial x| + |\partial u/\partial y| + |\partial u/\partial z| + |\partial v/\partial x| + |\partial v/\partial y| + |\partial v/\partial z| + |\partial w/\partial x| + |\partial w/\partial y| + |\partial w/\partial z|$$

We term the total distortion metric, S_1, as "total hydraulic strain" because it intrinsically conveys an awareness of the underlying distortion mechanisms of (2) linear deformation (whose tensor metric components are normal strain rates), (3) rotation (whose tensor metric components are angular velocities), and (4) angular deformation (whose tensor metric components are one-half the true shearing strain rates). Although rotation is not due to normal or shearing strain rates, the same spatial velocity gradients induce both angular deformation (shearing strain) and rotation. Mathematically, the magnitude of a 3D second rank tensor (matrix) may also be calculated as the Frobenius norm:

$$S_2 = \mathrm{SQRT}[\Sigma(\partial u_i/\partial x_j)^2] = \mathrm{SQRT}[(\partial u/\partial x)^2 + (\partial u/\partial y)^2 + (\partial u/\partial z)^2 + (\partial v/\partial x)^2 + (\partial v/\partial y)^2 + (\partial v/\partial z)^2 + (\partial w/\partial x)^2 + (\partial w/\partial y)^2 + (\partial w/\partial z)^2]$$

The Frobenius norm is the Euclidean norm for matrices and defines its size, length, or magnitude. The Euclidean norm for a 3D vector (a first rank tensor) is the familiar "square root of the sum of the squares" equation for calculating velocity magnitude from constituent velocity vectors. Calculating the distortion metric as the Frobenius norm, S_2, may be preferable and provide better results in future research, but for now the use of S_1 is considered sufficient since a comparison of S_1 and S_2 metrics (Figure 1) show the metrics have a linear relationship at the scale of our analyses. Also, loss of information due to the steady-state assumption in our CFD model data sets likely supersedes the differences between S_1 and S_2. In future time-variant CFD model simulations S_2 could be evaluated as a distortion metric.

Mechanisms (2) and (4) can be combined to form a single deformation quantity, i.e. the strain rate tensor ε_{ij}, whose diagonal components are the normal strain rates and off-diagonal components are one-half the true shearing strain rates. Spatial velocity gradients can then be viewed as inducing the mechanisms of deformation (described using the strain rate tensor) and rotation (described using the rotation or angular velocity tensor) (Figure 2).

Relationship between flow field distortion and river geomorphology

The importance of flow field distortion and implementation of the strain–velocity–pressure (SVP) hypothesis is best explained in the context of river geomorphology. In natural rivers, distortion of the flow field may be generally described as resulting from either (1) friction resistance producing wall-bounded flow occurring when a solid boundary (e.g. river channel) exerts skin or grain resistance on moving water and (2) form resistance producing free-shear flow occurring when bed form changes such as an obstruction in the flow (e.g. stump or rock outcrop) produce a local constriction in the flow area (Yang *et al.* 2005). Information contained in the total hydraulic strain and velocity fields is sufficient to separate structures producing friction resistance and form

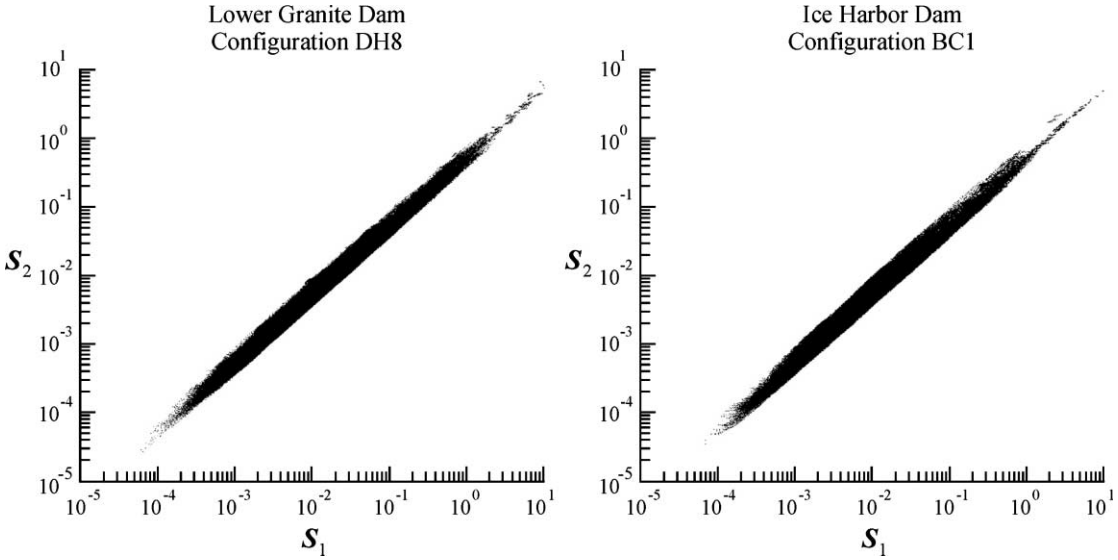

Figure 1 | Comparison of the distortion metric (total hydraulic strain) using two different calculation methods, S_1 (simplified) and S_2 (the Frobenius norm), at all nodes in the CFD model meshes for Lower Granite Dam configuration DH8 and Ice Harbor Dam configuration BC1 in Goodwin *et al.* (2006).

resistance flows. Wall-bounded flow gradients, associated with friction resistance, exhibit increasing total hydraulic strain and decreasing water velocity towards a solid boundary. In contrast, free-shear flow gradients, associated with form resistance, exhibit increasing total hydraulic strain and water velocity towards the obstruction. The pressure component of the SVP hypothesis recognizes that migrants generally change depth at a rate related more to their ability to adjust swim bladder volume than their vertical swimming velocity (Strand *et al.* 2005). Within the Numerical Fish Surrogate model (NFS), we consider these hydrodynamic cues to be environmental agents that interact with the fish agent.

Agent-based and behavioral modeling

According to the SVP hypothesis, information from the total hydraulic strain and velocity fields within range of the

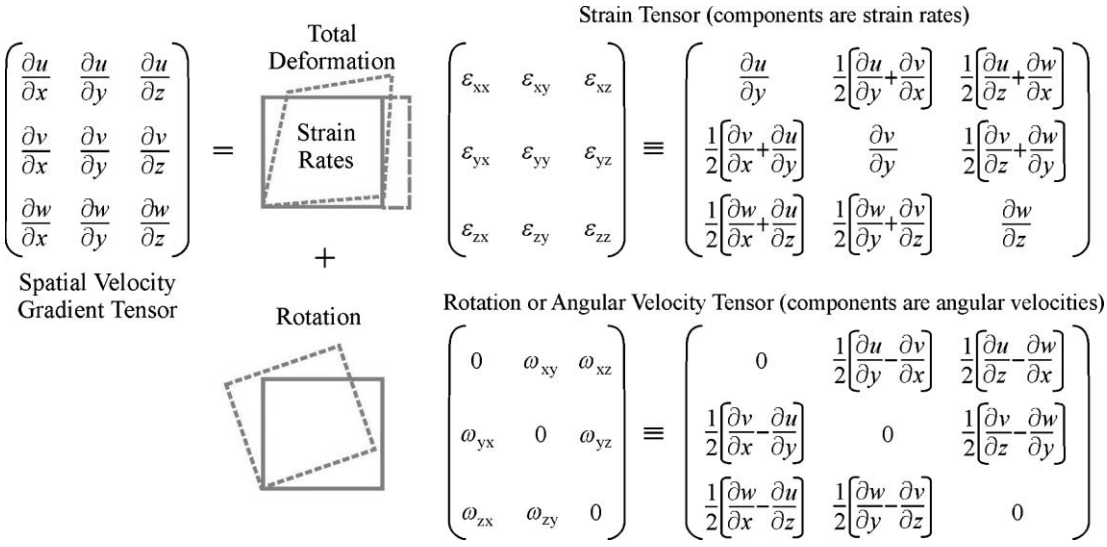

Figure 2 | The pure strain and shear strain tensors describing linear and angular deformation, respectively, can be combined into a single "strain rate" tensor ε_{ij} describing total deformation.

fish's sensory system provide cues about spatial distortion in the flow field sufficient for effective swim path selection. We simulate migrant swim path selection behavior as a response to one of four agents as identified by their hydraulic signature: (A_0) default agent in the absence of rheotactic cues, (A_1) wall-bounded flow gradient when the change in perceived total hydraulic strain exceeds threshold k_1, (A_2) free-shear flow gradient when the change in perceived total hydraulic strain exceeds threshold k_2, where $k_2 >> k_1$, and (A_3) pressure (hydrostatic) gradient when the change in perceived depth exceeds threshold k_3. In response to the agents the following behaviors are specified: (B_0) swimming with the flow vector, (B_1) swimming towards increasing water velocity to minimize total hydraulic strain, (B_2) swimming towards decreasing water velocity or against the flow vector to minimize total hydraulic strain, and (B_3) swimming towards acclimated pressure (depth). Swimming speed is bounded above by a burst speed of approximately 10 body lengths per second and below by the nominal cruising speed of approximately 2 body lengths per second (Beamish 1978). Fish orientation and speed for each time increment are described by the specified behavior B_i plus a random component. An agent-based, event-driven algorithm (Anderson 2002) is used to govern the hierarchy of potential responses emerging from multiple cues. Movement is mathematically implemented by adding the oriented speed response (volitional swim vectors) to a Lagrangian particle-tracking algorithm dynamically linked to a 3D Eulerian computational fluid dynamics (CFD) model as described in Goodwin *et al.* (2006). Implementing the SVP hypothesis requires accuracy in both the velocity and total hydraulic strain fields, unlike many CFD applications that require accuracy in predominantly the velocity field. The accuracy of forecast simulation to support fish bypass design will be sensitive to CFD options and mesh topologies, as discussed hereafter.

CFD model software and mesh topologies

A CFD model's internal solver determines whether it can be applied to either structured or unstructured meshes, or both. A structured mesh consists entirely of 8-node hexahedral elements for 3D problems and 4-node quadrilateral elements for 2D problems. These elements are arranged in an array with implicit order. An unstructured mesh consists of 4-node tetrahedral, 6-node wedge, 8-node hexahedral, or a combination of these elements for 3D problems; and 3-node triangles and 4-node quadrilateral elements for 2D problems. In an unstructured mesh, elements have no implicit order. A mesh may be composed of elements arranged into separate blocks of elements. If all blocks are structured meshes, the overall mesh is called a structured multi-block mesh. If any block is an unstructured mesh, the overall mesh is unstructured. Unstructured meshes are composed of all unstructured mesh blocks and an unstructured hybrid mesh is composed of a mix of structured and unstructured meshes.

In this application we use the general purpose, non-hydrostatic 3D CFD model U^{2}RANS developed at IIHR-Hydroscience & Engineering (Lai *et al.* 2003*a*, *b*) to provide the numerical hydrodynamic simulations. U^{2}RANS solves the 3D Reynolds-averaged Navier–Stokes (RANS) equations, and the mass and momentum equations are expressed concisely in Cartesian tensor form as follows:

$$\frac{\partial(\rho U_j)}{\partial x_j} = 0 \tag{1}$$

$$\frac{\partial(\rho U_i)}{\partial t} + \frac{\partial(\rho U_i U_j)}{\partial x_j} = -\frac{\partial P}{\partial x_i} + \frac{\partial}{\partial x_j}\left(\mu \frac{\partial U_i}{\partial x_j} - \rho\overline{u_i u_j}\right) \tag{2}$$

where U = mean velocity; u = fluctuating velocity; P = piezometric pressure; x_j =Cartesian coordinates; t = time; ρ = water density; μ = dynamic viscosity; and $-\rho\overline{u_i u_j}$ = Reynolds stress. A turbulence model is required to close the equations because of the appearance of the Reynolds stress, and the standard k–ε model (Launder & Spalding 1974) with wall functions is used in this study. The Reynolds stresses are related to the mean strain rate through an eddy viscosity as follows:

$$-\rho\overline{u_i u_j} = \mu_t\left(\frac{\partial U_i}{\partial x_j} + \frac{\partial U_j}{\partial x_i}\right) - \frac{2}{3}\rho k \delta_{ij} \tag{3}$$

and the eddy viscosity is obtained from

$$\mu_t = C_\mu \rho \frac{k^2}{\varepsilon} \tag{4}$$

where k = turbulence kinetic energy, ε = turbulence dissipation rate, and δ_{ij} =Kronecker symbol ($= 1$ when $i = j$,

otherwise = 0). The transport equations for k and ε are

$$\frac{\partial(\rho U_j k)}{\partial x_j} = \frac{\partial}{\partial x_j}\left[\left(\mu + \frac{\mu_t}{\sigma_k}\right)\frac{\partial k}{\partial x_j}\right] + G - \rho\varepsilon \quad (5)$$

$$\frac{\partial(\rho U_j \varepsilon)}{\partial x_j} = \frac{\partial}{\partial x_j}\left[\left(\mu + \frac{\mu_t}{\sigma_\varepsilon}\right)\frac{\partial \varepsilon}{\partial x_j}\right] + C_{\varepsilon 1}\frac{\varepsilon}{k}G - C_{\varepsilon 2}\rho\frac{\varepsilon^2}{k} \quad (6)$$

where $G = -\rho\overline{u_i u_j}(\partial U_i/\partial x_j)$ =generation of turbulence kinetic energy. The turbulence model coefficients are: $C_\mu = 0.09$, $\sigma_k = 1.0$, $\sigma_\varepsilon = 1.3$, $C_{\varepsilon 1} = 1.44$, and $C_{\varepsilon 2} = 1.92$.

The finite volume method preserves local and global conservation properties and is used to integrate the equations over a three-dimensional control volume using the Gauss Theorem. The key step in the finite volume method is the integration of the equations over each 3D control volume (computational cell). Then the volume integration terms are converted by the Gauss Theorem into surface integration over all faces composing the control volume. The remaining task in discretization is to appropriately express the convective, diffusive fluxes, and source terms on each face of the control volume. Technical details of the discretization and the solution procedure can be found in Lai *et al.* (2003*a*).

Calculating spatial velocity gradients (derivatives) in a CFD model

The nine spatial velocity gradients of $\partial u_i/\partial x_j$ must first be determined to calculate "total hydraulic strain". The nine spatial velocity gradients are actually spatial velocity derivatives because they represent the instantaneous rates of spatial change in velocity at any point in the flow field, i.e. gradients over an infinitesimal distance. Information in a CFD model is finite and output only at discrete locations. The gradient interval can be no smaller than that of a given mesh element (computational cell). The spatial velocity derivatives can be approximated in a number of ways but we limit our discussion here to the finite volume method because it is compatible with any finite volume based CFD model software and because it was used to calculate the spatial velocity derivatives for the applications described in this paper as well as those in Goodwin *et al.* (2006). We anticipate CFD models based on the finite element method can develop an equivalent spatial velocity derivative calculation method. The finite volume method is applicable to either structured or unstructured element meshes and calculates the spatial velocity derivatives for each individual mesh element without using inter-element "smoothing". Therefore, structure, gradation, and quality of the mesh determine whether the numerical solution of the spatial velocity derivatives exhibits continuity, i.e. the derivatives would not appreciably change or improve with a finer mesh. No calculation method can create a continuous solution field in the derivatives (i.e. justifiably smooth out large jumps in derivative values between elements) after the mesh is finalized – if the spatial velocity derivatives do not already exhibit continuity. Fundamental laws of physics stipulate that for sub-critical flow the spatial velocity derivatives exhibit neither jumps nor discontinuities.

Here we employ a finite volume method for estimating the spatial velocity derivatives using a hexahedral control volume consisting of the hexahedral mesh element itself. The calculation method uses the Divergence, or Gauss', theorem, to relate the rate of spatial change of velocity over the control volume to the geometrical property of the volume faces and the velocity values at the centers of each volume face. The adaptations needed for other mesh element types (e.g. tetrahedrons, etc.) should be readily apparent to a CFD modeler.

Concepts of divergence can be applied to the entire 3D vector (flow) field (i.e. u, v, and w in all three x, y, and z directions) to calculate spatial derivatives as well as the flux of an individual quantity (e.g. the vertical velocity w) in a particular (e.g. y) direction. Noting that in our example of the hexahedral control volume (mesh element) information on all variables is stored at the center, a spatial velocity derivative $\partial u_i/\partial x_j$ can be calculated on a volume-averaged basis at the control volume center by averaging the values of that particular spatial velocity derivative over the volume. This involves integrating the divergence of u_i in the x_j direction over the volume, then dividing by the control volume. The Divergence (or Gauss') Theorem simplifies this process by stating that integrating the vector field's divergence over the interior of the volume is equivalent to integrating the vector field over the volume's surface boundary. The complicated volume integral of divergence can be transformed into a much simpler surface integral which is then used to solve the equation.

Calculating spatial velocity gradients (derivatives) with U^{2}RANS

U^{2}RANS employs a unique procedure to define an arbitrary element face shape to calculate the surface area and volume of the mesh element (computational cell). The first step is to define the face center point, *C*, by taking the arithmetical average of the *N* vertices of the full surface. Then, by connecting point *C* with each vertex, *N* triangles are formed. These *N* triangles uniquely define the face shape. Geometric quantities such as element volume, face area, and face unit normal vector can then be calculated based on this definition. The area and surface normal vector of each triangle are easily computed by using the cross product of the position vectors (from the surface center point *C* to the vertices). The surface vectors of all triangles are then summed to obtain the surface normal vector for the whole computational cell face. The same approach is applied to other cell faces of the control volume. The volume of the computational cell is calculated using the Gauss Theorem:

$$\begin{aligned} V_{CV} &= \frac{1}{3}\int_{\partial V} \nabla \bullet \left(x\vec{i} + y\vec{j} + z\vec{k}\right) dv \\ &= \frac{1}{3}\left(\int_S x\vec{i} \bullet \vec{n} ds + \int_S y\vec{j} \bullet \vec{n} ds + \int_S z\vec{k} \bullet \vec{n} ds\right) \\ &= \frac{1}{3}\left(\sum_f x_f A_f^x + \sum_f y_f A_f^y + \sum_f z_f A_f^z\right) \end{aligned} \tag{7}$$

where x_f, y_f, z_f are the surface center coordinates, and A_f^x, A_f^y, A_f^z are the *x*-, *y*-, and *z*-components of the surface area vector.

Values of the variables for each Eulerian mesh node are calculated by averaging values at the control volume centers surrounding the mesh node. As an alternative, distance from the control volume center to the mesh node can be used as a weighting factor to allow for the fact that a smaller distance has a greater influence on the node value.

Developing CFD model meshes

Mesh quality is well known to affect both efficiency and accuracy of a CFD model solution for complex boundaries and flow patterns and is often considered more important than the numerical solution method or the particular CFD package used. Tessellation of a domain into discrete elements and equation discretization is applied to many different equations to analyze many different engineering problems including fluid, soil, and solid dynamics. In a numerical analysis, accuracy of a discretized solution can be no greater than that afforded by the corresponding continuous solution. A continuous governing equation can be, and often is, simplified even before equation discretization according to assumptions and simplifications that can be made in order to be compatible with the underlying system dynamics and the spatio-temporal scales of the analysis. Simplifications in the continuous equations impact the intrinsic accuracy of the analysis and cannot be mitigated with tessellation (i.e. increased mesh resolution). Tessellation of an entire domain into small elements that meet or perhaps even exceed (i.e. are smaller than) the scale of spatial accuracy afforded by the corresponding continuous equation is rarely possible because computer resources are finite. The practical goal of tessellation is to develop a mesh containing a limited number of discrete points that yields a solution exhibiting sufficient continuity (i.e. the solution would not appreciably improve with a finer mesh). Tessellation of a domain with a limited number of discrete points is well regarded as the stage where the modeler has the largest impact on solution accuracy and is arguably the most difficult and least straightforward stage in modeling.

Ensuring a high quality mesh

Criteria for developing a high quality mesh are not straightforward even though mesh development is the stage where the CFD modeler has the largest impact on solution quality. Ideally, meshes are composed of hexahedral (8-node) elements that are orthogonal (i.e. each element corner is 90°), distributed in the physical domain in such a way that all gradients are represented adequately, and oriented with the direction of flow. When complex geometries are involved non-uniform meshes must be used. A high quality non-uniform mesh satisfies criteria in attributes such as element size, element-to-element size variation, aspect ratio, skewness, smoothness, and boundary resolution. Development of a mesh is not straightforward since some criteria depend on boundary geometry, flow field complexity, and the type of hydrodynamic output needed. Also, tradeoffs in mesh and element

attributes are often necessary to run the CFD model within available computer resources In fact, constructing an appropriate mesh requires *a priori* knowledge of the solution – which usually is not known and the very reason for numerical simulation in the first place. Hence, the solution procedure often becomes iterative.

Attributes of high quality meshes

Developing an accurate flow field solution when derived quantities are needed is even more difficult, e.g. when spatial velocity derivatives are needed for accurately forecasting fish movement. Although *in situ* measurements of all nine spatial velocity derivatives are not as readily available as velocity data, physical laws tell us that for sub-critical flow the spatial velocity derivatives (i.e. the rates of spatial change in velocity) in nature are continuous. Therefore, as with the primary variables, a high quality solution in the derivatives exhibits continuity (i.e. the solution would not appreciably improve or change with a finer mesh). Since differentiation intensifies variability of a function, discontinuities introduced as discretization error by domain discretization (tessellation) may become more evident in the spatial velocity derivatives that are not as readily apparent in the solution field of primary variables (Figure 3). The 'art' of tessellation involves designing meshes that provide solutions exhibiting continuity in both primary and derivative quantities. Theoretically, a mesh providing continuity in the derivatives is more likely to provide a better solution in the primary variables as well. In this way, continuity in derivative quantities such as the spatial velocity derivatives may be used as a measure of mesh quality. A high quality mesh is composed of elements

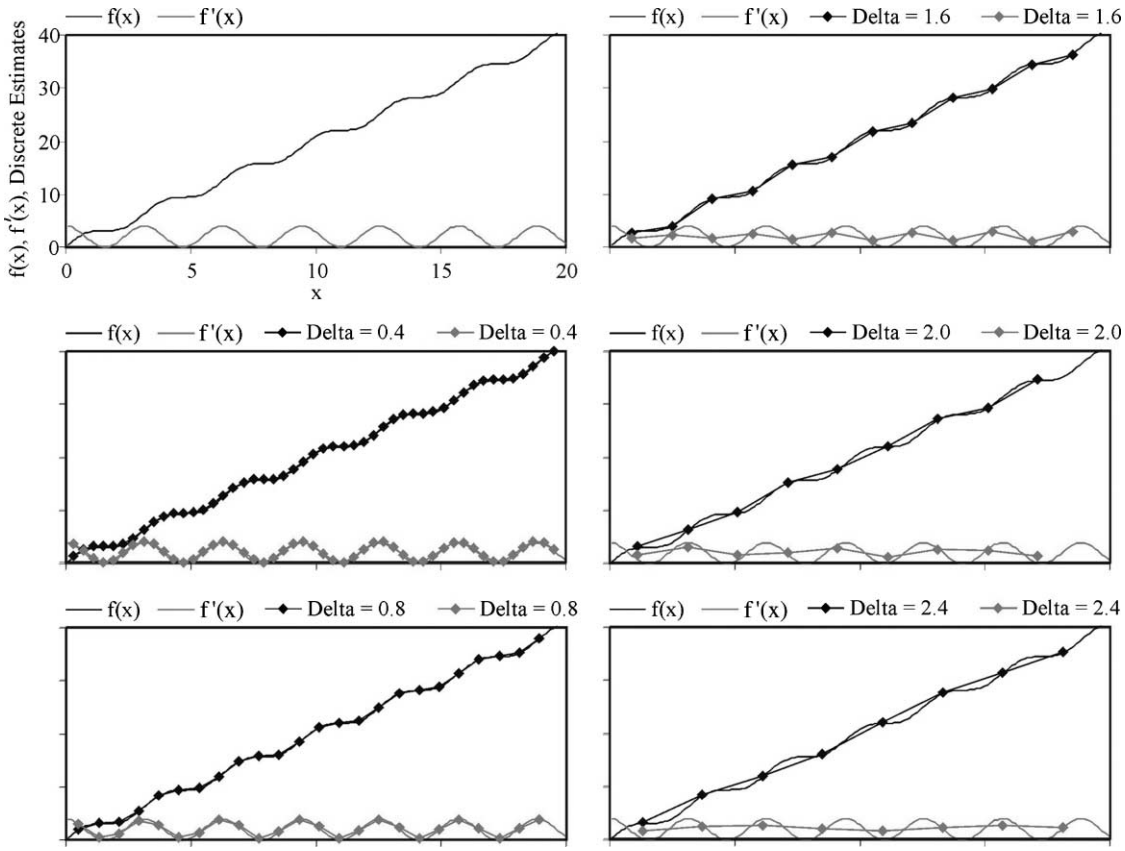

Figure 3 | Illustration of how mesh discretization impacts the ability to capture the trend in a primary, $f(x) = 2x + \sin(2x)$, and derivative, $f'(x) = 2 + 2\cos(2x)$, quantity with increasing discretization (delta value = 0.4, 0.8, 1.6, 2.0, 2.4). Increasingly courser discretization (surrogate for mesh quality) has a more deleterious impact on the ability to capture the trend in the derivative quantity. In a 3-D mesh, discontinuities introduced by domain discretization (tessellation) may be made more evident in the spatial derivatives of velocity that are not apparent in the solution field of primary variables. A high quality mesh provides a solution that would not appreciably improve or change with a finer mesh and is applicable to both primary and derivative quantities.

that satisfy criteria at both the local (individual element) and global levels. Once the flow field is determined the CFD modeler should ensure smaller mesh elements exist where velocity gradients are high to ensure a mesh-independent flow, which is particularly important for mesh elements adjacent to boundaries (Lane *et al.* 1999). Examples of good quality (for fish movement forecasting) boundary-fitted meshes are illustrated in Figures 4–7.

CFD modeled forebay hydrodynamics

The hydrodynamic environment encountered by migrant fish as they approach the Surface Bypass Collector (SBC, Figure 8) is shown in Figures 9–12. Changes of velocity V_M, total hydraulic strain, and acceleration in velocity direction a_D are small until about 10 m from the SBC when conditions begin to change significantly with maximum values occurring at the SBC entrances. Streamlines dive down in the region 100 m to 10 m from the SBC, then stabilize as they reach the dam. As streamlines pass under the trash boom (Figure 9) depth increases by about 1 m, velocity magnitude drops, and total hydraulic strain increases, but a_D remains essentially unchanged.

Acoustically-tagged (Figure 13) and numerically simulated virtual (Goodwin *et al.* 2006) migrants near the water surface move back and forth between the middle SBC entrance and the trash boom close to the powerhouse side but avoid areas near the Behavioral Guidance Structure (BGS, Figure 8). For comparison, 3D near-surface streamlines are plotted (in Figure 11) with associated hydrodynamic time-series of conditions plotted in Figure 12. The left-most streamline closest to the BGS slows to infinitesimal speed (essentially stops) as it approaches the BGS, indicating stagnant flow. However, the adjacent streamline dives deeper and enters the powerhouse intake. Some streamlines enter the BGS entrance and middle

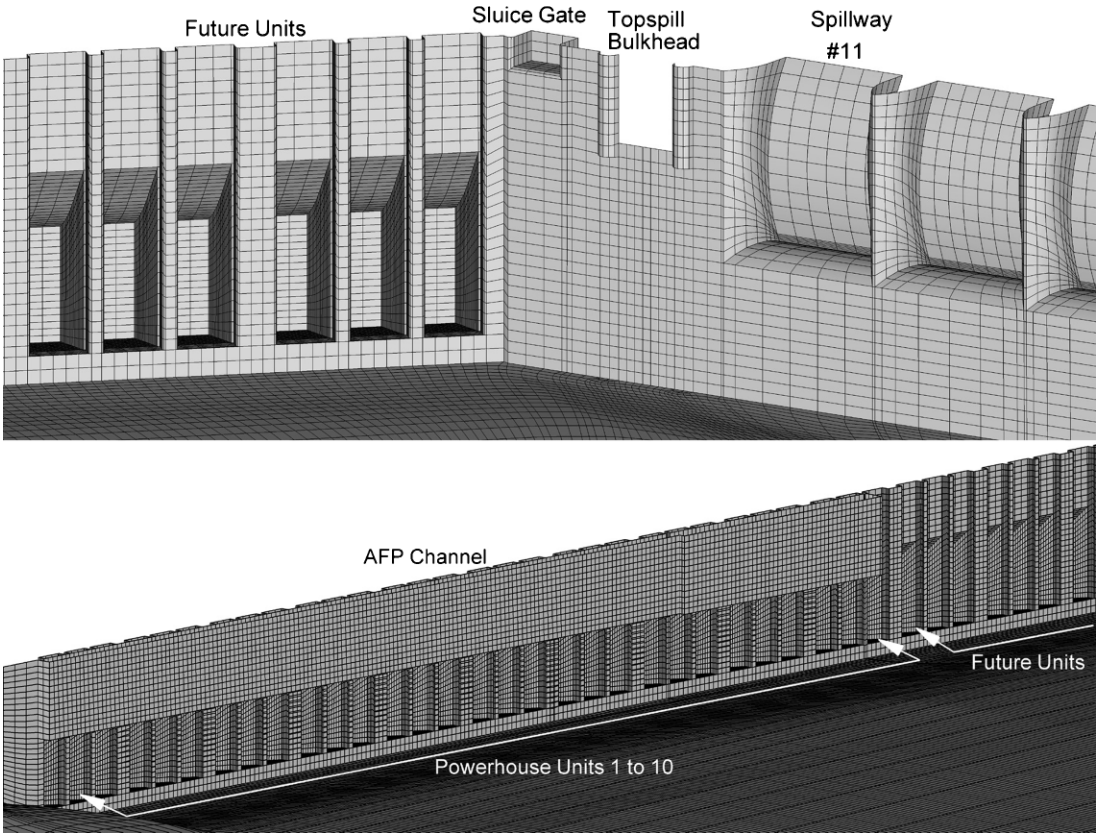

Figure 4 | Mesh topology for Topspill concept of fish passage at Wanapum Dam. The Topspill bulkhead is installed at spillbay 12 with an opening of 6.1 m high and 12.2 m wide. There are two 7.6 m high, semi-circular piers with a 1.2 m radius.

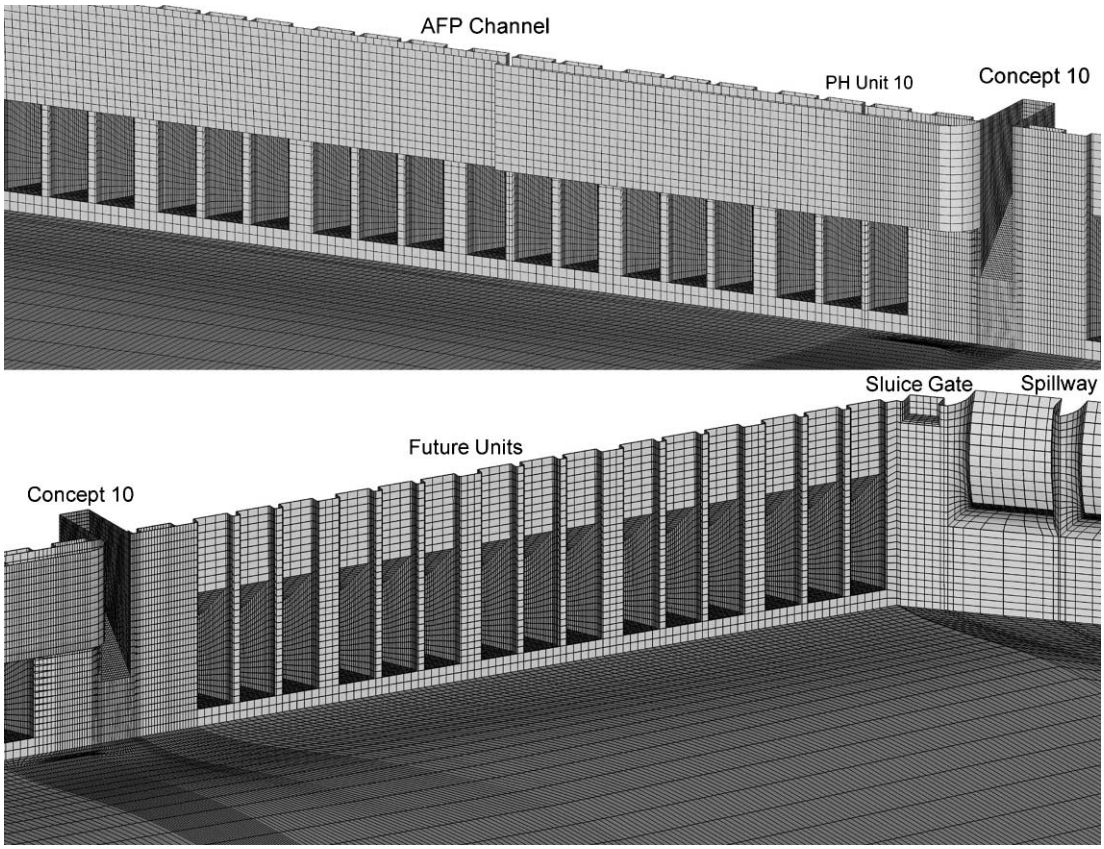

Figure 5 | Mesh topology for Concept 10 of fish passage at Wanapum Dam. Concept 10 is installed at the center intake of future powerhouse turbine unit 11. Entrance is 6.1 m wide, crest at elevation 167.8, 165.4, and 160.8 m (forebay water surface elevation is 173.74 m) for bypass flow discharges at 141.6, 283.2, and 566.3 cm, sill elevation at 148.2 m. Entrances of intakes located to the left and right of future unit 11 are closed.

entrance to the SBC, while others stop at the SBC. These changes in the hydrodynamic conditions start approximately 10 m from the SBC and may trigger a behavioral repertoire different from that executed further upstream.

AGENT-BASED MODEL CALIBRATION AND VALIDATION

The goal of the agent-based Numerical Fish Surrogate model developed here is a decision-support tool that can (i) forecast observed (measured) trends in fish passage proportions and (ii) rank fish bypass configurations by descending order of their measured passage proportions. The Numerical Fish Surrogate is calibrated with data from Lower Granite Dam forebay configuration DH8 (Figures 7 – 12). Calibration data include: (1) high resolution CFD model output to describe the forebay hydrodynamic pattern, (2) horizontal and vertical distributions of migrants entering the dam forebay, (3) detailed 3D tracks of individual acoustically-tagged fish migrants, and (4) proportions of fish entering the spillway, turbines, and bypass, respectively.

Calibration is a two-phase process. First, the behavior model coefficients (see Goodwin *et al.* 2006) are adjusted until individual virtual migrant tracks calculated at 2.0 s time increments qualitatively resemble movement patterns of acoustically-tagged migrants for configuration DH8. Next, coefficients are fined-tuned so that the passage proportions of 2000 virtual migrants released upstream quantitatively resemble the measured passage proportions through the bypass, spillway, and turbines for configuration DH8. The calibrated Numerical Fish Surrogate was then validated by comparing its output to measured passage proportions at 19 other configurations described in Goodwin *et al.* (2006)

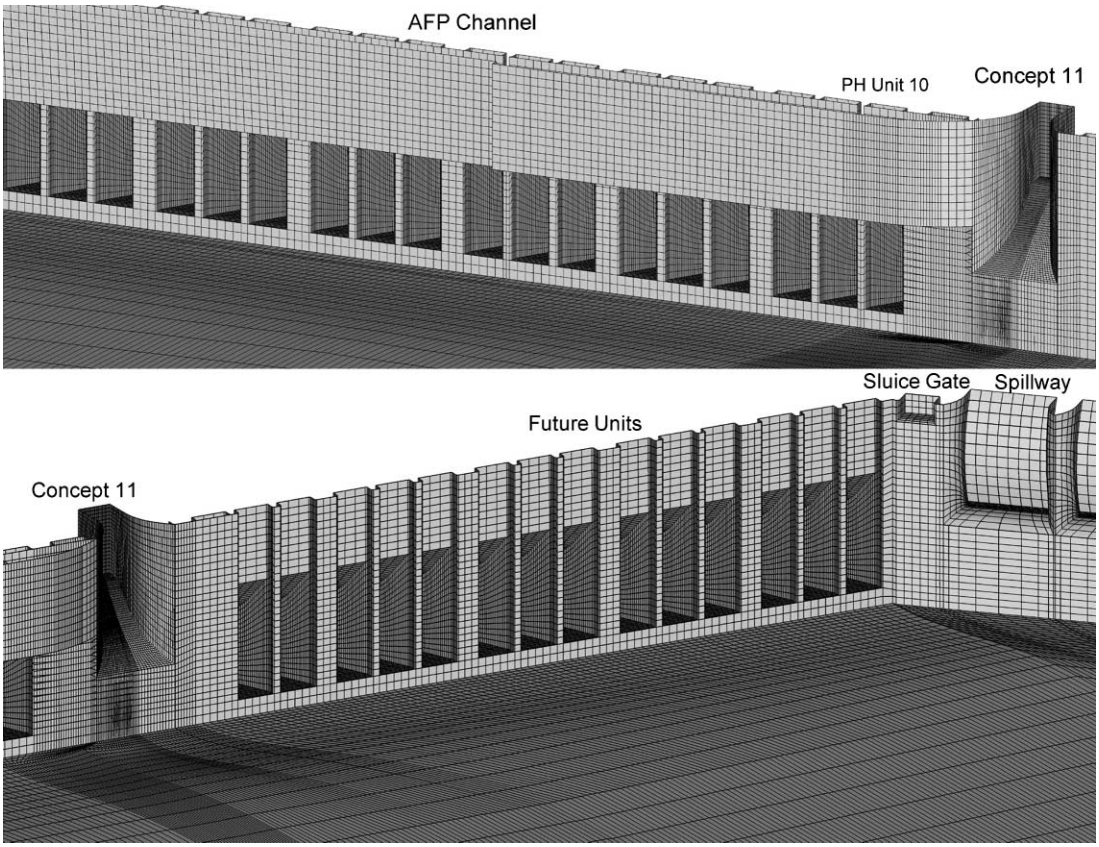

Figure 6 | Mesh topology for Concept 11 for fish passage at Wanapum Dam. Concept 11 is installed at the center intake of future powerhouse turbine unit 11. Entrance is 15.1 m wide and then transited to 6.1 m wide at the crest location, crest at elevation 168.6, 165.8, and 161.5 m (forebay water surface elevation is 173.74 m) for bypass flow discharges at 141.6, 283.2, and 566.3 cm, sill elevation at 148.7 m. Entrances of intakes located to the left and right of future unit 11 are closed.

including: 2 at Ice Harbor Dam, 5 at Wanapum Dam, and 12 at Lower Granite Dam. Improvements in the memory allocation of the Numerical Fish Surrogate permitted simulation of 5000 virtual migrants at this stage of the study. Forecasted passage proportions for the calibration configuration DH8 did not change substantially with the increase from 2000 to 5000 virtual migrants.

As described in detail in Goodwin *et al.* (2006), NFS forecasts generally match observed passage proportions with goodness of fit (slope/R-square) decreasing from spillway (0.95/0.85), bypass (1.07/0.80), to powerhouse (1.15/0.61). The reduced goodness of fit for the powerhouse is likely related to the difficulty of maintaining constant operation of the powerhouse during field studies when migrants were observed to pass the dam. Total powerhouse discharge usually remains constant, but the units in operation and the distribution of load across those units typically changes during a study period. In contrast, a steady-state CFD model does not capture changes in operation. Spillway operation is held constant during a test and, therefore, meets the steady-state assumption. Bypass system operation is also held constant, but its location nearer the powerhouse than the spillway for most cases probably reduces its goodness of fit. Turning the behavioral rules off (passive transport) reduces the goodness of fit (slope/R-square) of the spillway to 0.49/0.50, bypass 0.10/0.10, and powerhouse 0.24/0.08 (Goodwin *et al.* 2006). Improvement in goodness of fit provided by the rules represents the contribution of the behavioral rules towards the quality of the forecasts.

FORECASTING PASSAGE RESPONSE OF MIGRANTS TO ALTERNATIVE ENGINEERING DESIGNS

We present here an application of the ELAM method, the Numerical Fish Surrogate, for the design of juvenile fish

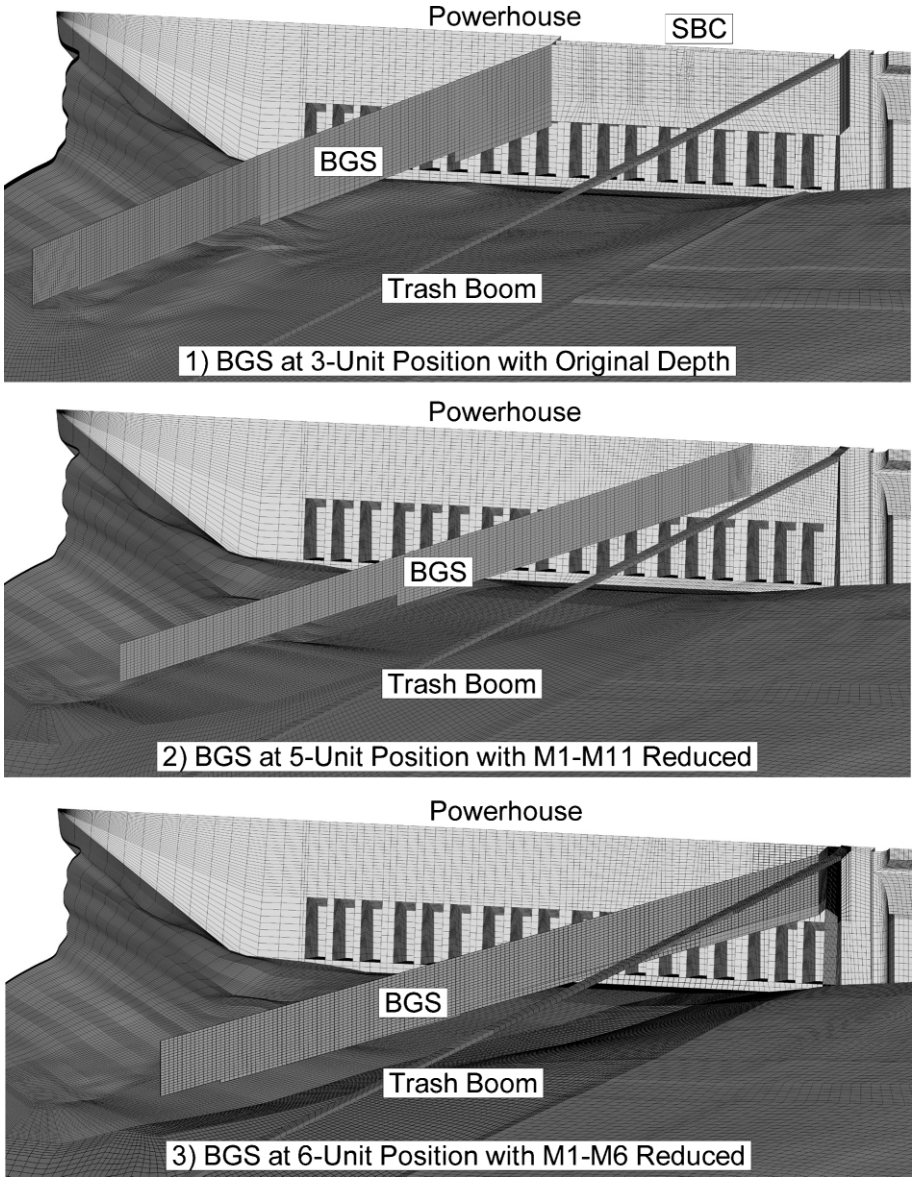

Figure 7 | Mesh topology for Lower Granite Dam forebay. Alternative BGS alignments are depicted with 3-, 5-, and 6-unit occlusion positions illustrated from top to bottom and with the original, M1–M11, and M1–M6 reduced depth configurations, respectively. The SBC is removed when BGS alternatives at the 5- or 6-unit occlusion positions are evaluated.

passage facilities at Wanapum Dam. This example embodies all of the mesh quality and CFD modeling guidelines described above. Wanapum Dam is located at river mile 415 on the Columbia River in Washington State. It is owned and operated by Public Utility District No. 2 of Grant County, Washington (the District). The District has been evaluating fish passage concepts to achieve 95% survival of downstream migrating juvenile salmonids (migrants) at Wanapum Dam. To assist with this evaluation, three-dimensional (3D) computational fluid dynamics (CFD) models have been developed by IIHR-Hydroscience & Engineering for the forebay and tailrace of Wanapum Dam. As a mainstem project on the mid-Columbia River, Wanapum Dam has endeavored to develop a future unit bypass for migrants (Jacobs *et al.* 2003). IIHR has developed CFD models and conducted numerical simulations to assist in locating and sizing the bypass opening. The developed CFD model for Wanapum Dam was first compared to field

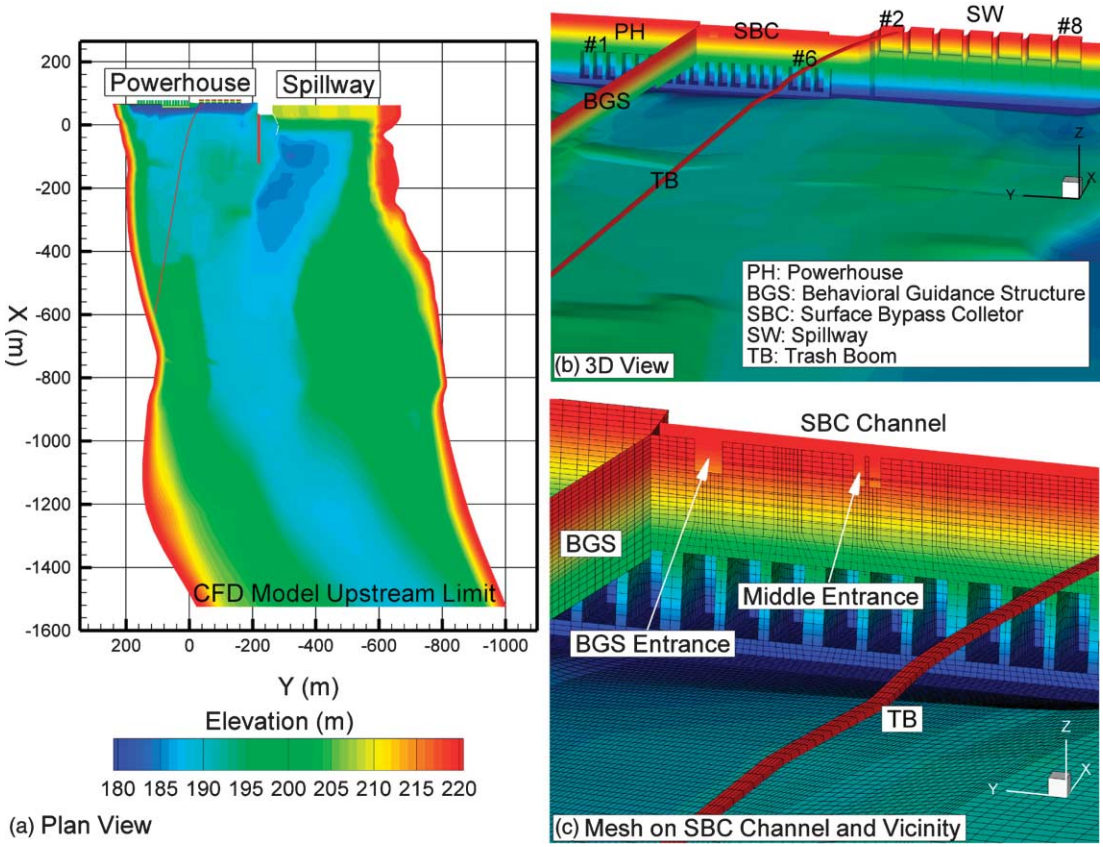

Figure 8 | Configuration DH8 (Goodwin *et al.* 2006) used to calibrate coefficients of the Numerical Fish Surrogate. Plan view of the CFD model boundary domains with elevation contours. 3D view of the configuration showing the 6 powerhouse units, 8 spillbays (bay 1 was occupied by the conduit connecting the SBC to the spillway), Behavioral Guidance Structure (BGS), Surface Bypass Collector (SBC), and trash boom (TB). Close-up view near the SBC with the CFD model mesh. SBC has two openings marked as BGS entrance and middle entrance.

data (Li & Weber 2006*a*). It was then used in the studies on fish passage alternatives at Wanapum Dam (Jacobs *et al.* 2003). Among these fish passage alternatives, the CFD model was used to examine the hydrodynamic characteristics associated with three historical non-turbine passage routes for which there were fish passage data and to compare the three historical routes with a conceptual fish passage route located immediately adjacent to the powerhouse (Li & Weber 2006*b*). Modeling was undertaken to examine the hydrodynamics associated with a range of bypass flows and different structural bypass configurations located near the powerhouse. Following a review of the results and consultation with resource agency participants, the focus was on developing and assessing concepts with a maximum bypass flow of 20 kcfs and more modeling to examine the hydrodynamics associated with three basic 20 kcfs concepts (Li & Weber 2006*c*). Finally, the fish bypass was selected for future unit 11. Regulating gates were included in the design to permit bypass discharges of 5, 10, and 20 kcfs, with several transitions from the Attraction Flow Prototype (AFP) channel to the future unit bypass pier (Li & Weber 2006*d*).

Numerical Fish Surrogate coefficients calibrated at Lower Granite Dam on the Snake River were used at Wanapum Dam without modification because acoustic-tag data, normally used for calibration/re-calibration, were not available at Wanapum Dam prior to this stage in project planning. Virtual fish movement and passage behavior patterns based on the Lower Granite Dam behavior coefficients were compared directly to measured (radio-tagged fish) passage proportions at Wanapum Dam for the 2002 MOA spill configuration (Table 1). After determining adequacy of the initial comparison, the NFS model was applied "as is" to the four additional scenarios in Table 1.

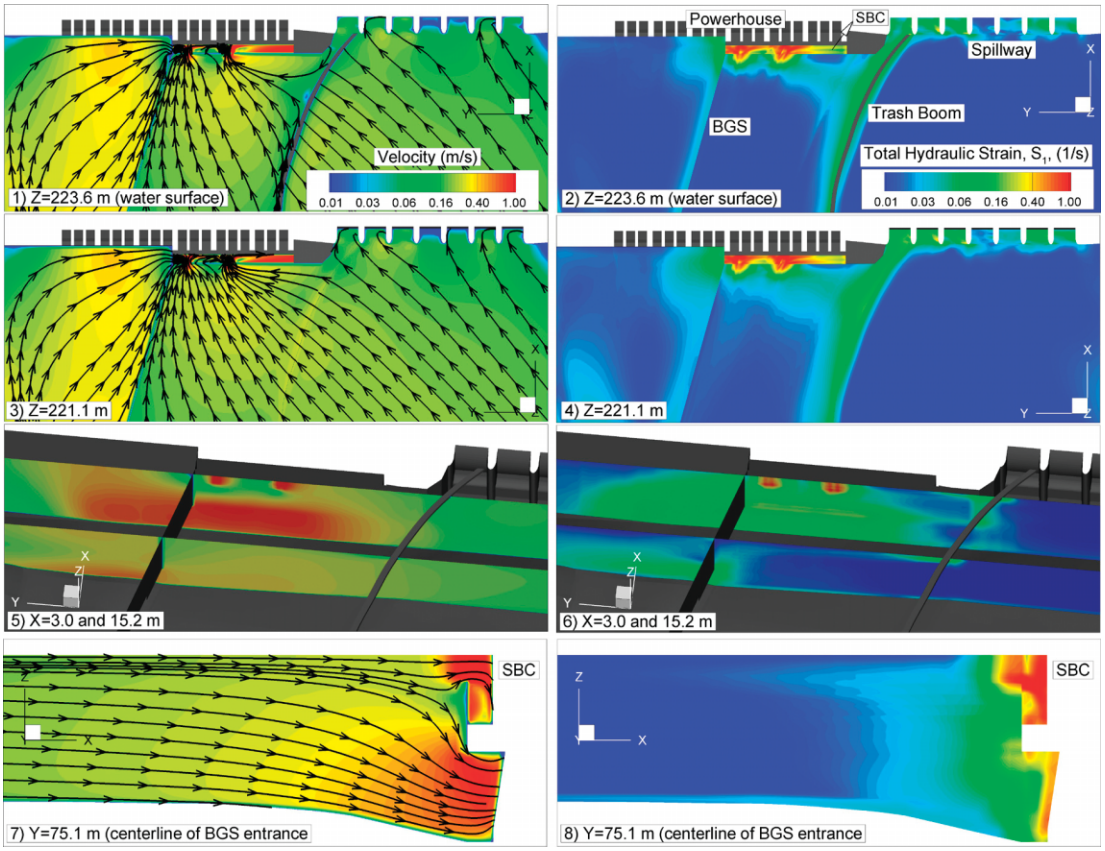

Figure 9 | Velocity magnitude and streamlines (left plots) and total hydraulic strain for configuration DH8. Plan view slice taken at $z = 223.6$ m (water surface) and $z = 221.1$ m, lateral cross-sectional slice (parallel to dam face) taken at $x = 3.0$ m (10 ft upstream of the SBC) and $x = 15.2$ m (50 ft upstream of the SBC), and longitudinal cross-sectional slice (perpendicular to dam face) taken through centerline of BGS entrance of the SBC ($Y = 75.1$ m).

The NFS model results generally follow similar patterns with relatively little difference for all three virtual fish release groups (day, night, and composite) (Goodwin *et al.* 2005). Forecast fish passage proportions with 5000 and 2000 virtual fish and 5000 passive particles are listed in Table 1. About 15% of the virtual fish remain in the forebay at the termination of each NFS run (Goodwin *et al.* 2005). For more effective comparison, these remaining fish were apportioned to each exit route assuming the same proportions as previously passed virtual fish. The forecasted passage closely matches observed passage. Results for passages with behavior rules on are in considerably better agreement with the observed passage than the fit for passive particles (behavior rules off). We define the fish passage efficiency as the ratio of fish passage percentage (proportion) over the flow percentage passing the exit route. Observed and forecasted results indicate surface bypasses (such as the top spill bulkhead, sluice gate) have considerably higher passage efficiency than the spillway and turbines. The efficiency of the spillway is comparable to that of turbines, which suggests that a near-surface exit route with proper location and configuration can greatly increase the fish passage efficiency at Wanapum Dam. Both observed and forecasted results reveal that the Attraction Flow Prototype (AFP) channel is an inefficient route for fish passage despite being a surface-oriented collector. This suggests the NFS model distributes the fish not based on whether the exit route is a surface versus non-surface route, but instead based on fundamental process-based behavior dynamics that underlie the observed passage patterns.

After review and evaluation of the comparisons, and approval from the District, the NFS model was applied to forecast plausible migrant response to alternative designs of the fish passage facility. The Topspill (Figure 4), Concept 10

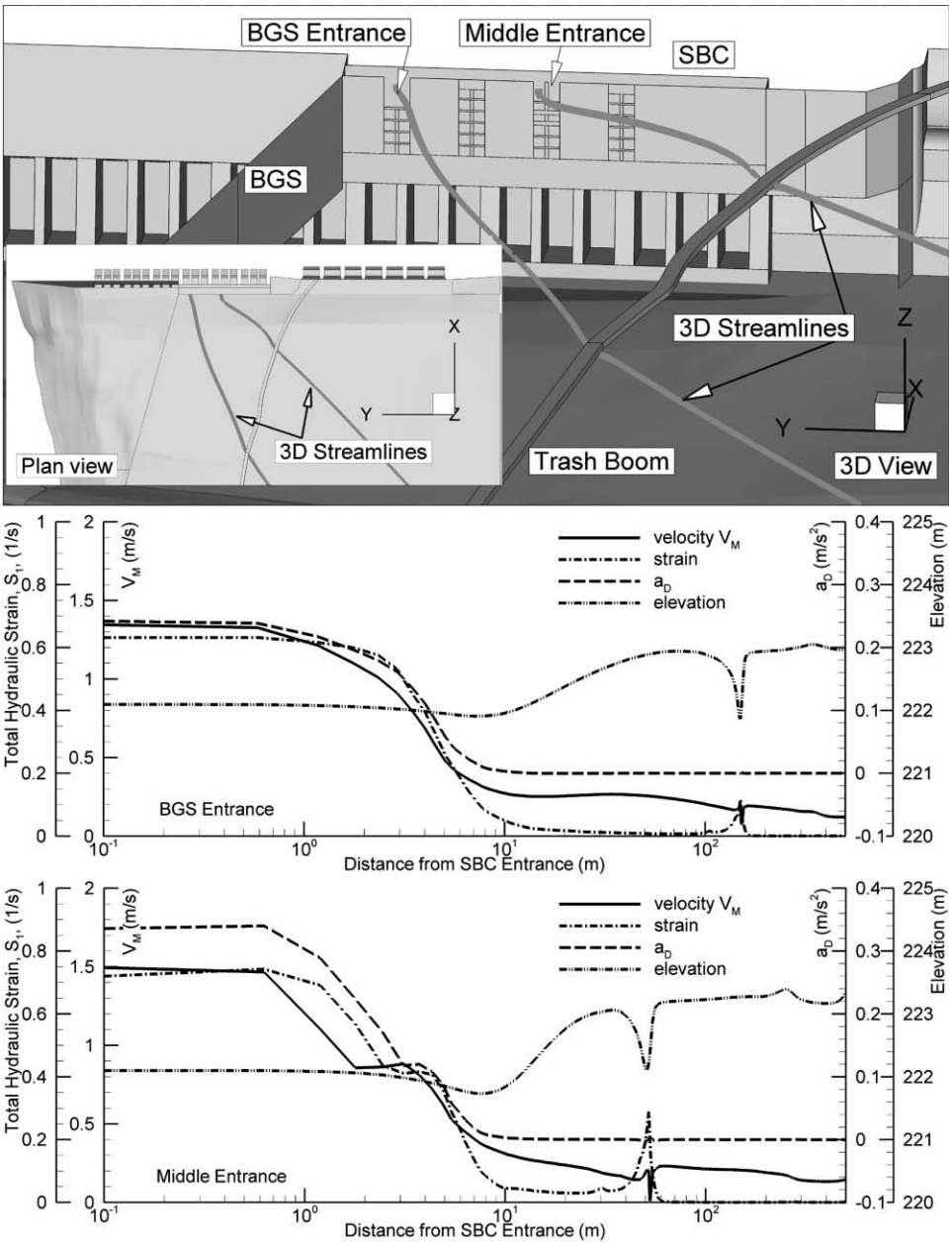

Figure 10 | Hydrodynamic features along 3D streamlines entering SBC entrances for Lower Granite Dam configuration DH8. 3D streamlines released at centerline of BGS entrance and left half of the middle entrance at 1.52 m (5 ft) below the water surface and tracked back into forebay. Upper frame shows the plan and 3D views of streamlines. Middle and lower frames show velocity magnitude V_M, total hydraulic strain, acceleration in velocity direction a_D, and elevation along the 3D streamlines entering the BGS entrance and middle entrance. a_D is defined as $a_D = V_i a_i / V_M$ and represents the status of acceleration ($a_D > 0$) or deceleration ($a_D < 0$), V_i is the velocity component, and a_i is the acceleration component of flow. Distance is the distance from the entrance along the x direction of the CFD model, which corresponds to the direction perpendicular to the dam face.

(Figure 5), and Concept 11 (Figure 6) were modeled and compared, and the flow conditions and forecasted fish passage proportions are as listed in Table 2. Detailed flow and operational conditions for these cases and the corresponding hydrodynamic flow patterns can be found in Li & Weber (2006*d*). Concepts 10 and 11 exhibit similar hydrodynamic patterns as represented by the streamlines, velocity magnitude contours, total hydraulic strain at 1.5 m depth plane (Figure 14). However, the construction cost of Concept 11 was estimated to be approximately 30% higher

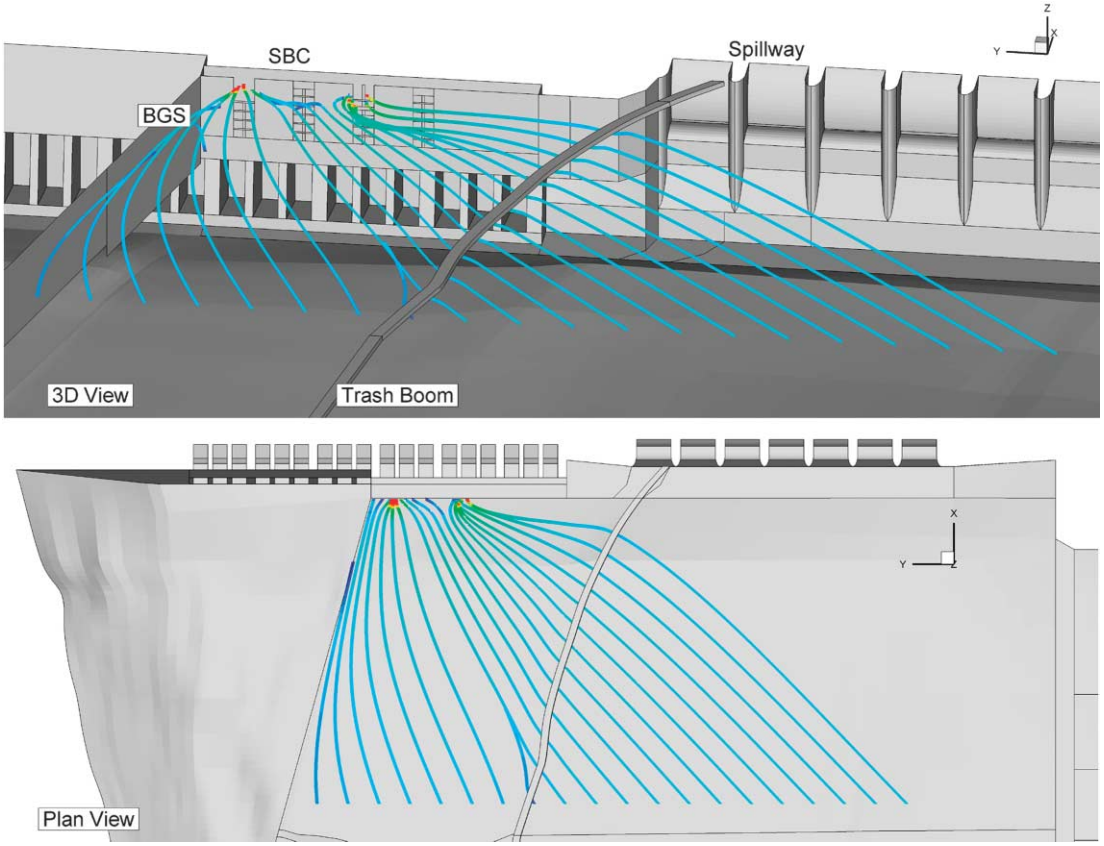

Figure 11 | 3D and plan views of near-surface streamlines for Lower Granite Dam configuration DH8.

than Concept 10. This increase is due to the wider entrance of Concept 11 and the necessity to remove an intermediate pier in future unit 11.

Forecasted fish passage results for different concepts are compared in Table 2. We can draw the following conclusions from the results: (1) when fish passage flow increases from 141.6 cm to 283.2 cm Concept 10 does not respond with an increase in fish passage proportion while Concept 11 increases roughly by 2.5%. When flow increases to 566.3 cm both Concepts 10 and 11 have about a 9% increase in fish passage proportion; (2) Concept 11 exhibits slightly higher fish passage proportions than Concept 10 at 283.2 cm and 566.3 cm, but slightly lower at 141.6 cm bypass flow; and (3) both Concepts 10 and 11 have higher fish passage proportions than Topspill Concept by about 3.5%.

Given the similar fish passage characteristics, hydrodynamic signature in the forebay and increased construction cost of Concept 11, the design team in consultation with the resources agencies chose to advance Concept 10 to final design and construction.

DISCUSSION

Results from this research on developing an agent-based Numerical Fish Surrogate model suggest: (1) the NFS model can help detect seriously flawed design alternatives, such as the Attraction Flow Prototype (AFP) channel entrance which should deter more fish than the more favorable future unit fish bypass or Topspill bulkhead entrances; (2) while near-surface exit routes tend to exhibit considerably higher fish passage efficiency, turbines and spillway remain comparable; (3) the future unit fish bypass is able to attract flow from a wider region and produce higher fish passage proportions than the Topspill bulkhead; and (4) application

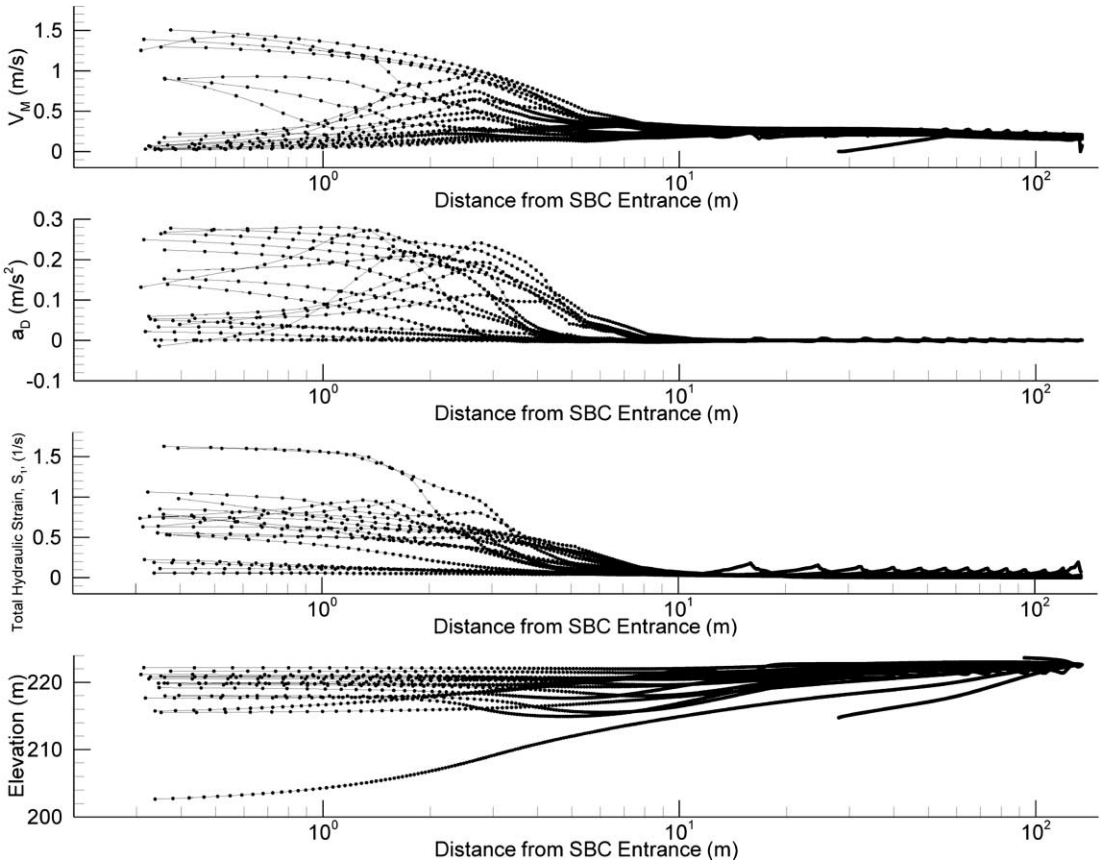

Figure 12 | Hydrodynamic features along the 3D near-surface streamlines in Figure 11 for Lower Granite Dam configuration DH8. Note the variation of velocity magnitude, acceleration in velocity direction, total hydraulic strain, and elevation along the streamlines.

of the Numerical Fish Surrogate model exhibits a bright perspective in engineering practices related to fish passage. We developed the model not only as one part of project evaluation (as was used in this project), but also to develop an understanding of bypass dynamics sufficient to identify opportunities for additional cost-effective design or operational improvements (Stedinger 2000).

Benchmarking CFD methods, software, and meshes for the NFS

Few standards exist in CFD modeling. Different CFD model solution methods, software, and meshes (e.g. layout, element density, and gradation) may provide equally accurate, but different, depictions of the flow field because of differences in the intrinsic idiosyncrasies and biases of the CFD model tool used. Developing Numerical Fish Surrogate (NFS) coefficients immune to the magnitude of idiosyncrasies and biases presently observed among different CFD modeling tools is neither possible nor desirable because it would effectively de-sensitize the Numerical Fish Surrogate to the same subtle flow field characteristics used to elicit virtual migrant movement behavior. Instead, for future applications of the NFS with other CFD modeling tools we propose a benchmarking of the different CFD model solution methods, software, and meshes using velocity magnitude and total hydraulic strain, S_1, as reference indicators. Benchmarking velocity is important to ensure that approach flow fields are modeled consistently. Benchmarking total hydraulic strain is important near any water–surface interface and critical for two additional reasons. First, differences in compared flow field solutions will be most evident in the spatial velocity derivatives. Second, consistent and accurate spatial velocity derivatives, such as S_1, exhibiting continuity (i.e. no mesh-induced discretization error) are critically important to

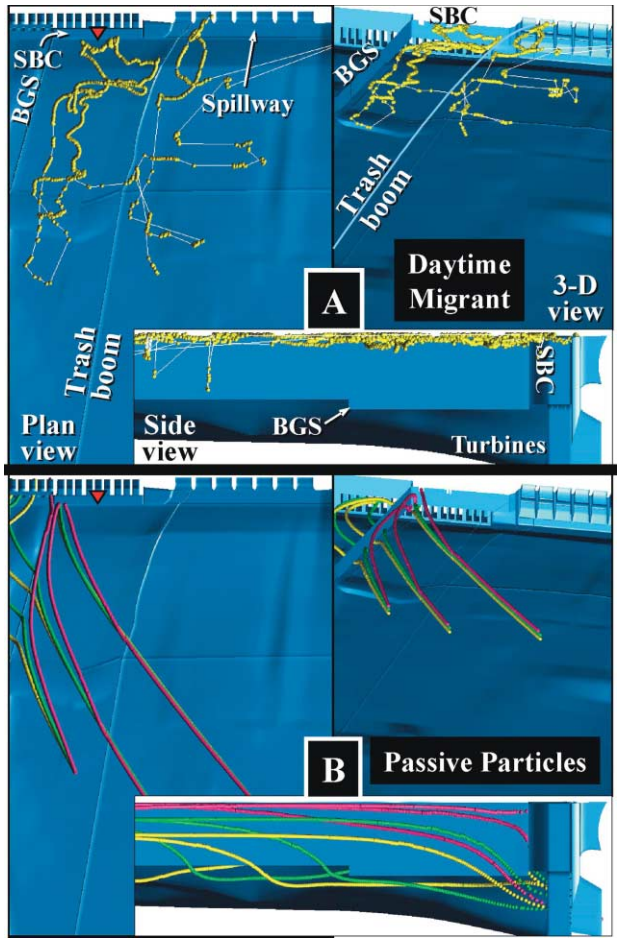

Figure 13 | Forebay of Lower Granite Dam on the Snake River, WA, USA with (A) near-surface acoustically-tagged migrant movement pattern observed at Lower Granite Dam for configuration DH8 and (B) nine neutrally buoyant passive particles released 1 m (purple), 5 m (green), and 10 m (yellow) below water surface indicating flow lines for configuration DH8. Fish entering the Surface Bypass Collector (SBC) are conveyed into spillbay 1 nearest the powerhouse. Middle entrance of the SBC indicated with red triangle. The Behavioral Guidance Structure (BGS) is intended to guide migrants into the bypass (SBC). The BGS is a suspended steel wall approximately 24.4 m deep at its intersection with the powerhouse and tapers in step-wise manner to a minimum of 16.8 m at its upstream end. The trash boom is approximately a constant 1.2 m deep. Acoustic-tag data from Cash *et al.* (2002).

Numerical Fish Surrogate analyses. Benchmarking will allow different CFD model solution methods, software, and meshes to be used with the Numerical Fish Surrogate and provide consistent decision-support of similar accuracy.

Benchmarking velocity magnitude and streamlines

Benchmarking velocity magnitude (V_M) is implemented by calculating V_M for a designated project and configuration with great flow complexity using the new CFD model solution method, software, or mesh topology. We suggest a minimum of one designated configuration (i.e. Lower Granite Dam configuration DH8) and, preferably, two configurations (both modeled using the U^{2}RANS structured mesh and finite volume method, which was used to calibrate the Numerical Fish Surrogate). Velocity magnitude, V_M, for the designated configuration(s) based on the U^{2}RANS structured mesh and finite volume method is subtracted from velocity magnitude calculated from the new CFD model solution method, software, or mesh topology. Assuming steady mean flow conditions (in which case streaklines from multiple particle releases correspond to streamlines), streamlines released uniformly, laterally and vertically, at the upstream boundary for the designated configuration(s) based on the U^{2}RANS structured mesh and finite volume method are compared to similarly obtained streamlines for the new CFD model solution method, software, or mesh topology. Velocity magnitude differences greater than 0.03 to 0.04 m/s and streamlines approaching different parts of the dam in different proportions should be rectified.

Benchmarking total flow field distortion (total hydraulic strain)

The CFD model for configuration DH8 was used to calibrate the coefficients of the Numerical Fish Surrogate. Also, the first in a series of validation simulations (19 validation simulations in Goodwin *et al.* (2006)) used the same spatial velocity derivative calculation method as configuration DH8. Benchmarking total hydraulic strain is implemented by calculating S_1 for a designated project and configuration with great flow complexity using the new CFD model solution method, software, or mesh topology. The configuration(s) used to benchmark velocity magnitude are also used to benchmark total hydraulic strain. Total hydraulic strain, S_1, for the designated configuration(s) based on the U^{2}RANS structured mesh and finite volume method is subtracted from total hydraulic strain, S_1, calculated from the spatial velocity derivatives of the new CFD model solution method, software, or mesh topology. The difference is plotted using 3D slices, a log scale with range $1^{E\text{-}9}$ to 1, and color fill contours matching those of the designated configurations (e.g. DH8 in Goodwin *et al.* (2006)). Differences should be rectified.

Table 1 | Comparison of observed and forecasted fish passage at Wanapum Dam

			NFS forecasted passage % (efficiency)		
Routes	**Flow, cms (% of total)**	**Observed passage % (efficiency)** *	**5000 fish**	**2000 fish**	**5000 passive particles**
Case 2002-MOA					
Bypass	–	–	–	–	–
Sluice gate	53.8 (1.3)	6.9 (5.3)	7.5 (5.8)	8.8 (6.8)	0.8 (0.6)
Turbines	2602.3 (62.8)	58.4 (0.9)	56.6 (0.9)	56.8 (0.9)	43.9 (0.7)
Spillway	1486.6 (35.9)	33.7 (0.9)	35.9 (1.0)	34.4 (1.0)	55.3 (1.5)
Case 1997-AFP					
3Bypass	39.6 (0.6)	1.0 (1.8)	0.0 (0.0)	0.1 (0.2)	0.5 (0.9)
Sluice gate	62.3 (0.9)	2.0 (2.3)	3.1 (3.6)	3.2 (3.7)	0.1 (0.1)
Turbines	4281.5 (59.4)	36.0 (0.6)	51.7 (0.9)	50.6 (0.9)	41.1 (0.7)
Spillway	2828.9 (39.2)	61.0 (1.6)	45.2 (1.2)	46.1 (1.2)	58.4 (1.5)
Case 2001					
Bypass	–	–	–	–	–
Sluice Gate	48.1 (2.6)	40.2 (15.6)	31.4 (12.2)	35.9 (14.0)	2.1 (0.8)
Turbines	1212 (64.8)	32.3 (0.5)	63.0 (1.0)	59.6 (0.9)	47.6 (0.7)
Spillway	611.6 (32.7)	24.5 (0.7)	5.7 (0.2)	4.6 (0.1)	50.3 (1.5)
Case 2002-Mixed					
Bypass	367 (8.4)	26.7 (3.2)	24.6 (2.9)	25.4 (3.0)	13.3 (1.6)
Sluice gate	–	–	–	–	–
Turbines	3032.7 (75.6)	56.6 (0.7)	65.8 (0.9)	65.0 (0.9)	56.2 (0.7)
Spillway	640 (16.0)	14.7 (0.9)	9.6 (0.6)	9.5 (0.6)	30.5 (1.9)
Case 2002-Topspill					
Bypass	345.5 (8.3)	17.9 (2.2)	15.5 (1.9)	15.2 (1.8)	17.7 (2.1)
Sluice gate	–	–	–	–	–
Turbines	3811.4 (91.7)	91.1 (1.0)	84.3 (0.9)	84.7 (0.9)	82.2 (0.9)
Spillway	0.0	0.0 (0.0)	0.0 (0.0)	0.0 (0.9)	0.0 (0.0)

*Observed (radio-tagged fish) passage proportions from Robichaud *et al.* (2005).

Table 2 | Forecasted fish passage for alternative designs at Wanapum Dam

	Configurations	Bypass	Sluice gate	Turbines	Spillway
Flow rate, cms	Topspill @ 566.3	566.3	0	3256.4	0
	Concept 10 @ 141.6	141.6	0	3681.2	0
	Concept 10 @ 283.2	283.2	0	3539.6	0
	Concept 10 @ 566.3	566.3	0	3256.4	0
	Concept 11 @ 141.6	141.6	0	3681.2	0
	Concept 11 @ 283.2	283.2	0	3539.6	0
	Concept 11 @ 566.3	566.3	0	3256.4	0
Forecasted passage % 5000 virtual fish	Topspill @ 566.3	23.5	0	76.5	0
	Concept 10 @ 141.6	18.0	0	82.0	0
	Concept 10 @ 283.2	18.1	0	81.9	0
	Concept 10 @ 566.3	26.9	0	73.1	0
	Concept 11 @ 141.6	16.3	0	83.7	0
	Concept 11 @ 283.2	18.8	0	81.2	0
	Concept 11 @ 566.3	27.1	0	72.9	0
Forecasted passage efficiency	Topspill @ 566.3	1.59	0	0.90	0
	Concept 10 @ 141.6	4.87	0	0.85	0
	Concept 10 @ 283.2	2.45	0	0.88	0
	Concept 10 @ 566.3	1.82	0	0.86	0
	Concept 11 @ 141.6	4.40	0	0.87	0
	Concept 11 @ 283.2	2.54	0	0.88	0
	Concept 11 @ 566.3	1.83	0	0.86	0

Mitigating differences and the need for benchmarking

Mitigating differences may involve counter-balancing idiosyncrasies and biases in any new CFD solution method or software with "calibration" until it mathematically replicates and exhibits the same biases and idiosyncrasies in velocity, streamlines, and especially the spatial velocity derivatives as the U^2RANS structured mesh and finite volume method used in this study. For instance, it may be found that elements of different types (i.e. tetrahedrons) might need to be packed or graded differently than otherwise needed to describe the flow field similarly to the U^2RANS structured mesh and

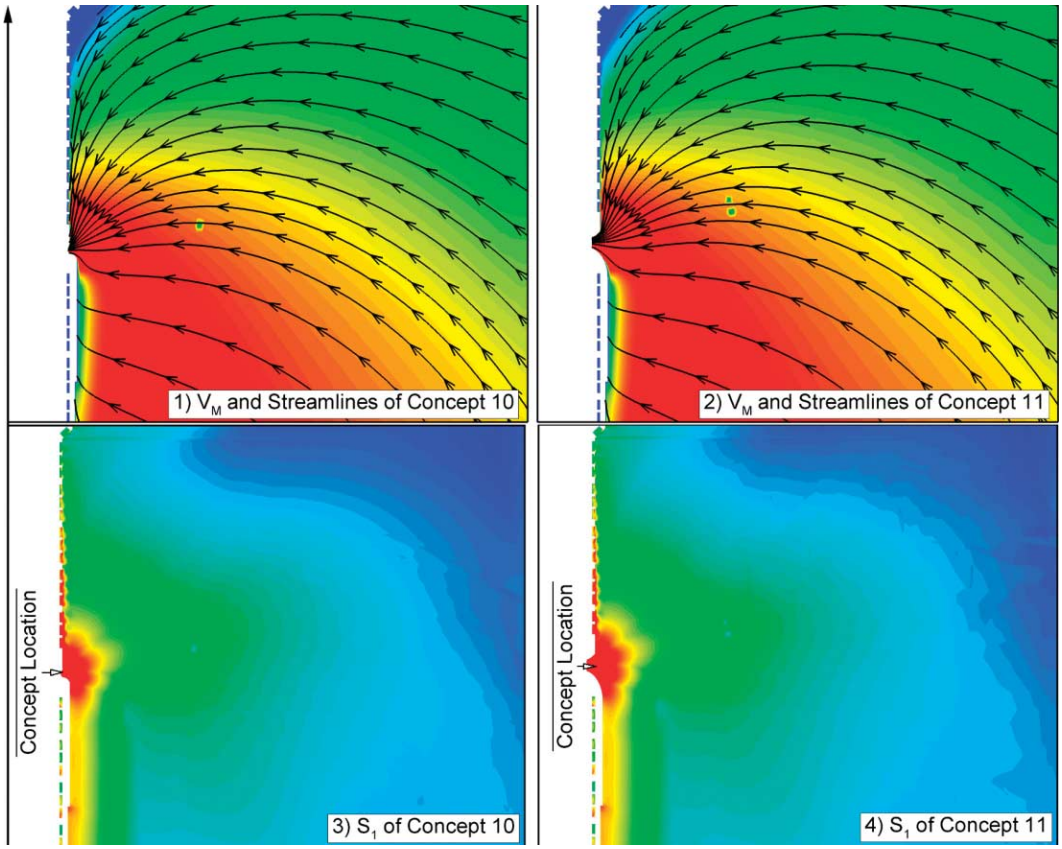

Figure 14 | Streamlines, velocity magnitude (V_M), and total hydraulic strain (S_1) contours at 1.52 m depth plane in the near field for Concepts 10 and 11 for Wanapum Dam.

finite volume method. These guidelines are ported and applied to other projects and configurations needing a CFD modeled data set. Benchmarking is needed until the state-of-the-art in CFD modeling sufficiently advances to the point where the intrinsic idiosyncrasies and biases of different CFD modeling tools, resulting in different subtle flow field characteristics to which the Numerical Fish Surrogate is sensitive, are no longer an issue. The need for benchmarking has emerged from past experience where new CFD model methods, software, and meshes representing the same river conditions and dam structural and operational configuration exhibited significant differences in the velocity magnitude and total hydraulic strain patterns compared to the U^{2}RANS simulation.

If a high quality mesh already exists (i.e. the solution would not appreciably change or improve with a finer mesh) and no "calibration" of the intrinsic idiosyncrasies and biases of the new CFD model tool (i.e. compared to the U^{2}RANS structured mesh and finite volume method) is pursued, the Numerical Fish Surrogate model must be re-calibrated to the spatial velocity derivatives calculated using the different CFD model solution method, software, or mesh. This greatly limits the intended purpose of the Numerical Fish Surrogate to serve as a management decision-support tool for identifying opportunities for cost-effective intervention to improve system operation. The intended purpose of the Numerical Fish Surrogate as a regional, mathematical knowledge base requires the porting of coefficients (ie representing fish-flow relationship information) and that it be applied with many different CFD models at many different projects. The benefit of a regional approach is evident from the Wanapum Dam application described in this paper.

Comparing and mitigating differences in the velocity magnitude, streamlines, and spatial velocity derivatives (total hydraulic strain) is straightforward and provides a much needed process for benchmarking hydrodynamic data sets, presently missing in hydraulic design of fish bypass systems and Numerical Fish Surrogate studies. This process sets clear and tractable benchmarks for applying different CFD model

solution methods, software, and mesh topologies and maintains consistency and integrity of the subtle hydrodynamic patterns to which the Numerical Fish Surrogate is calibrated. Otherwise, there is no theoretical or practical way to guarantee that intrinsic, systematic differences in the spatial velocity derivatives will not adversely impact fish simulation results and, more importantly, decision-support provided to sponsors. This study shows that advanced computational modeling approaches (numerical CFD simulation) can be blended with alternative hydroinformatics technologies (agent-based behavioral models for fish movements) to increase the predictive capabilities of decision support systems in eco-environmental applications.

ACKNOWLEDGEMENTS

The tests described and the resulting data presented herein, unless otherwise noted, were obtained from research conducted under the sponsorship of the US Army Engineer District Walla Walla, the Grant County Public Utility District, and the System-Wide Water Resources Program (SWWRP), a US Army Corps of Engineers research and development initiative. We gratefully acknowledge Lynn Reese and Mark Lindgren of Walla Walla District and Dana Jeske, Curt Dotson, and Joe Lukas of Grant County Public Utility District for their funding support and Ken Cash of the US Geological Survey for collecting and filtering the acoustic-tag data in Figure 13. 3D computer virtual fish animations and further information on Eulerian–Lagrangian–Agent methods (ELAMs) can be found at http://el.erdc.usace.army.mil/emrrp/nfs/. Permission was granted by the Chief of Engineers to publish this information.

REFERENCES

Anderson, J. J. 2002 An agent-based event driven foraging model. *Natural Res. Model.* **15** (1), 55–82.

Anderson, R. A. & Enger, P. S. 1968 Microphonic potentials from the sacculus of a teleost fish. *Compar. Biochem. Physiol.* **27**, 879–881.

Beamish, F. W. H. 1978 *Fish Physiology* volume VII *Locomotion*. (ed. Hoar W. S. & Randall D. J.). Academic Press. New York pp. 101–183.

Booker, D. J., Dunbar, M. J. & Ibbotson, A. 2004 Predicting juvenile salmonid drift-feeding habitat quality using a three-dimensional hydraulic-bioenergetic model. *Ecol. Model.* **177**, 157–177.

Cash, K. M., Adams, N. S., Hatton, T. W., Jones, E. C. & Rondorf, D. W. 2002 *Three-Dimensional Fish Tracking to Evaluate the Operation of the Lower Granite Surface Bypass Collector and Behavioral Guidance Structure during 2000*. Final Report prepared by the US Geological Survey Columbia River Research Laboratory for the US Army Corps of Engineers, Walla Walla District. Walla Walla, WA.

Coombs, S., Braun, C. B. & Donovan, B. 2001 The orienting response of Lake Michigan mottled sculpin is mediated by canal neuromasts. *J. Exp. Biol.* **204**, 337–348.

Coutant, C. C. 2001 Integrated, multi-sensory, behavioral guidance systems for fish diversions. In *Behavioral Technologies for Fish Guidance* (ed. C. C. Coutants), American Fisheries Society Press. Bethesda, MD, American Fisheries Society, Symposium 26, Bethesda, MD pp. 105–113.

Coutant, C. C. & Whitney, R. R. 2000 Fish behavior in relation to passage through hydropower turbines: a review. *Trans. Am. Fisheries Soc.* **129**, 351–380.

Gerolotto, F., Soria, M. & Freon, P. 1999 From two dimensions to three: the use of multi-beam sonar for a new approach to fisheries acoustics. *Can. J. Fisheries Aquatic Sci.* **56** (1), 6–12.

Goodwin, R. A. 2004 Hydrodynamics and juvenile salmon movement behavior at Lower Granite Dam: decoding the relationship using 3-D space-time (CEL Agent IBM) simulation. PhD Dissertation. Cornell University Ithaca, NY.

Goodwin, R. A., Nestler, J. M., Anderson, J. J., Kim, J. & Toney, T. 2005 *Evaluation of Wanapum Dam Bypass Configurations for Outmigrating Juvenile Salmon Using Virtual Fish: Numerical Fish Surrogate (NFS) Analysis*. ERDC/EL TR-05-7, US Army Engineer Research and Development Center. Vicksburg, MS.

Goodwin, R. A., Nestler, J. M., Anderson, J. J., Weber, L. J. & Loucks, D. P. 2006 Forecasting 3-D fish movement behavior using a Eulerian-Lagrangian-agent method (ELAM). *Ecol. Model.* **192**, 197–223.

Harden, B. (2003) The Pacific Northwest Hits Jackpot Of Salmon: Administration Critics, Supporters Disagree: Was It Skill or Luck? *The Washington Post*, 20 August, p A03.

Hudspeth, A. J. 1989 How the ear's works work. *Nature* **341**, 397–404.

Jacobs Civil Inc., IIHR-Hydroscience & Engineering & Oakwood Consulting Inc. 2003 *Fish Passage Alternatives Study for the Priest Rapids Project*. Final Report, Public Utility District No. 2 of Grant County, prepared by Jacobs Civil Inc. IIHR-Hydroscience & Engineering and Oakwood Consulting Inc.

Kalmijn, A. J. 1989 Functional evolution of lateral line and inner-ear sensory systems. In *The Mechanosensory Lateral Line: Neurobiology and Evolution* (eds Coombs S., Görner P. & Münz H.). Springer-Verlag. New York pp. 187–215.

Kalmijn, A. J. 2000 Detection and processing of electromagnetic and near-field acoustic signals in elasmobranch fishes. *Phil. Trans. R. Soc. Ser. B* **355** (1401), 1135–1141.

Kim, Y. -H. & Wardle, C. S. 2005 Basic modelling of fish behaviour in a towed trawl based on chaos in decision-making. *Fisheries Res.* **73**, 217–229.

Kröther, S., Mogdans, J. & Bleckmann, H. 2002 Brainstem lateral line responses to sinusoidal wave stimuli in still and running water. *J. Exp. Biol.* **205**, 1471–1484.

Lai, Y. G., Weber, L. J. & Patel, V. C. 2003a Nonhydrostatic three-dimensional model for hydraulic flow simulation. I: Formulation and verification. *J. Hydraul. Engng.* **129** (3), 196–205.

Lai, Y. G., Weber, L. J. & Patel, V. C. 2003b Nonhydrostatic three-dimensional model for hydraulic flow simulation. II: Validation and application. *J. Hydraul. Engng.* **129** (3), 206–214.

Lane, S. N., Bradbrook, K. F., Richards, K. S., Biran, P. A. & Roy, A. G. 1999 The application of computational fluid dynamics to natural river channels: three-dimensional versus two-dimensional approaches. *Geomorphology* **29**, 1–20.

Launder, B. E. & Spalding, D. B. 1974 The numerical computation of turbulent flows. *Comput. Meth. Appl. Mech. Engng.* **3**, 269–289.

Li, S. & Weber, L. J. 2006*a Comprehensive Comparison of the Three-Dimensional Computational Fluid Dynamics (CFD) Model Outputs with Field Data of the Wanapum Dam Forebay and Tailrace*. Submitted to Public Utility District No. 2 of Grant County, Ephrata, Washington 98823, Limited Distribution Report No 335, IIHR-Hydroscience & Engineering, College of Engineering, The University of Iowa. Iowa City, IA.

Li, S. & Weber, L. J. 2006*b A Comparison of Hydrodynamic Parameters Associated with Various Fish Passage Routes at Wanapum Dam*. Submitted to Public Utility District No. 2 of Grant County, Ephrata, Washington 98823, Limited Distribution Report No. 334, IIHR-Hydroscience & Engineering, College of Engineering, The University of Iowa. Iowa City, IA.

Li, S. & Weber, J. L. 2006*c Three-Dimensional (3-D) Computational Fluid Dynamics (CFD) Modeling of Fish Passage Through Various Bypass Routes at Future Units of Wanapum Dam*. Submitted to Public Utility District No. 2 of Grant County, Ephrata, Washington 98823, Limited Distribution Report No. 336, IIHR-Hydroscience & Engineering, College of Engineering, The University of Iowa. Iowa City, IA.

Li, S. & Weber, J. L. 2006*d Three-Dimensional Computational Fluid Dynamics Modeling of Fish Passage Through Various Bypass Routes at Wanapum Dam: For Numerical Fish Surrogate Analysis, Fish Passage Radio-telemetry Studies, and Future Unit Concept Assessment*. Submitted to Public Utility District No. 2 of Grant County, Ephrata, Washington 98823, Limited Distribution Report Draft, IIHR-Hydroscience & Engineering, College of Engineering, The University of Iowa. Iowa City, IA.

Lucas, M. C. & Baras, E. 2000 Methods for studying spatial behaviour of freshwater fishes in the natural environment. *Fish Fisheries* **1**, 283–316.

Montgomery, J. C., Carton, A. G., Voigt, R., Baker, C. F. & Diebel, C. 2000 Sensory processing of water currents by fishes. *Phil. Trans. R. Soc. Ser. B* **355** (1401), 1325–1327.

Montgomery, J. C., Coombs, S. & Halstead, M. 1995 Biology of the mechanosensory lateral line in fishes. *Rev. Fish Biol. Fisheries* **5**, 399–416.

Mynett, A. E. 2002 Environmental hydroinformatics: The way ahead. Key Note Address. In *Proceedings of the 5th International Conference on Hydroinformatics*, **vol. 1**, pp. 31–36. IWA Publishing Ltd. London, UK, Cardiff, UK, July 1-5.

Mynett, A. E., Chen, Q. N. & Babovic, V. M. 2004 Artificial intelligence techniques in environmental hydroinformatics: The role of expert knowledge. In *Proceedings of the 4th International Symposium on Environmental Hydraulics and 14th IAHR-APD Congress*, **vol. 1**, pp. 3–13. Hong Kong, December 15-18, 2004.

Neitzel, D. A., Dauble, D. D., Cada, G. F., Richmond, M. C., Guensch, G. R., Mueller, R. P., Abernethy, C. S. & Amidan, B. 2004 Survival estimates for juvenile fish subjected to a laboratory-generated shear environment. *Trans. Am. Fisheries Soc.* **133**, 447–454.

Nestler, J. M., Goodwin, R. AF., Smith, D. L. & Anderson, J. J. in press. Mathematical and conceptual framework for the new discipline of ecohydraulics. In *Hydroecology and Ecohydrology: Past, Present and Future.*(eds. Wood P. J., Hannah D. M. & Sadler J. P.), John Wiley & Sons.

Popper, A. N. & Carlson, T. J. 1998 Application of sound and other stimuli to control fish behavior. *Trans. Am. Fisheries Soc.* **127**, 673–707.

Robichaud, D., Nass, B., Timko, M. A., English, K. K. & Ransom, B. 2005 *Analysis of Smolt Behavior and Relative Survival at Wanapum Dam using Three-Dimensional Acoustic Telemetry, 2004*. Draft Report, prepared for Public Utility District No. 2 of Grant County, 19 January.

Rogers, P. H. & Cox, M. 1988 Underwater sound as a biological stimulus. In *Sensory Biology of Aquatic Animals* (ed. Atema J., Fay R. R., Popper A. N. & Tavolga W. N.), Springer-Verlag. New York pp. 131–149.

Stedinger, J. R. 2000 *The Use of Risk and Uncertainty Analyses Within the US Army Corps of Engineers Civil Works Programs*. Prepared for USACE Institute for Water Resources by Cornell University, Ithaca, NY.

Steel, E. A., Guttorp, P., Anderson, J. J. & Caccia, D. C. 2001 Modeling juvenile migration using a simple Markov chain. *J. Agric. Biol. Environ. Statist.* **6** (1), 80–88.

Steig, T. W. 1999 The use of acoustic tags to monitor the movement of juvenile salmonids approaching a dam on the Columbia River. (eds Eiler J. H., Alcorn D. J. & Neuman M. R.), *Biotelemtry 15: Proceedings of the 15th International Symposium on Biotelemetry, 9–14 May, Juneau, AK*. International Society of Biotelemetry. Wageningen, The Netherlands, pp. 296–304.

Strand, E., Jørgensen, C. & Huse, G. 2005 Modelling buoyancy regulation in fishes with swimbladders: bioenergetics and behaviour. *Ecol. Model.* **185**, 309–327.

Suckling, E. E. & Suckling, J. A. 1964 Lateral line as a vibration receptor. *J. Acoust. Soc. Am.* **36**, 2214–2216.

Turchin, P. 1997 Quantitative analysis of animal movements in congregations. In *Animal Groups in Three Dimensions* (eds. Parrish J. K. & Hamner W. M.), Cambridge University Press. New York pp. 107–112.

Voigt, R., Carton, A. G. & Montgomery, J. C. 2000 Responses of anterior lateral line afferent neurons to water flow. *J. Exp. Biol.* **203**, 2495–2502.

Yang, S. -Q., Tan, S. -K. & Lim, S. -Y. 2005 Flow resistance and bed form geometry in a wide alluvial channel. *Wat. Res. Res.* **41**, W09419.

APPENDIX

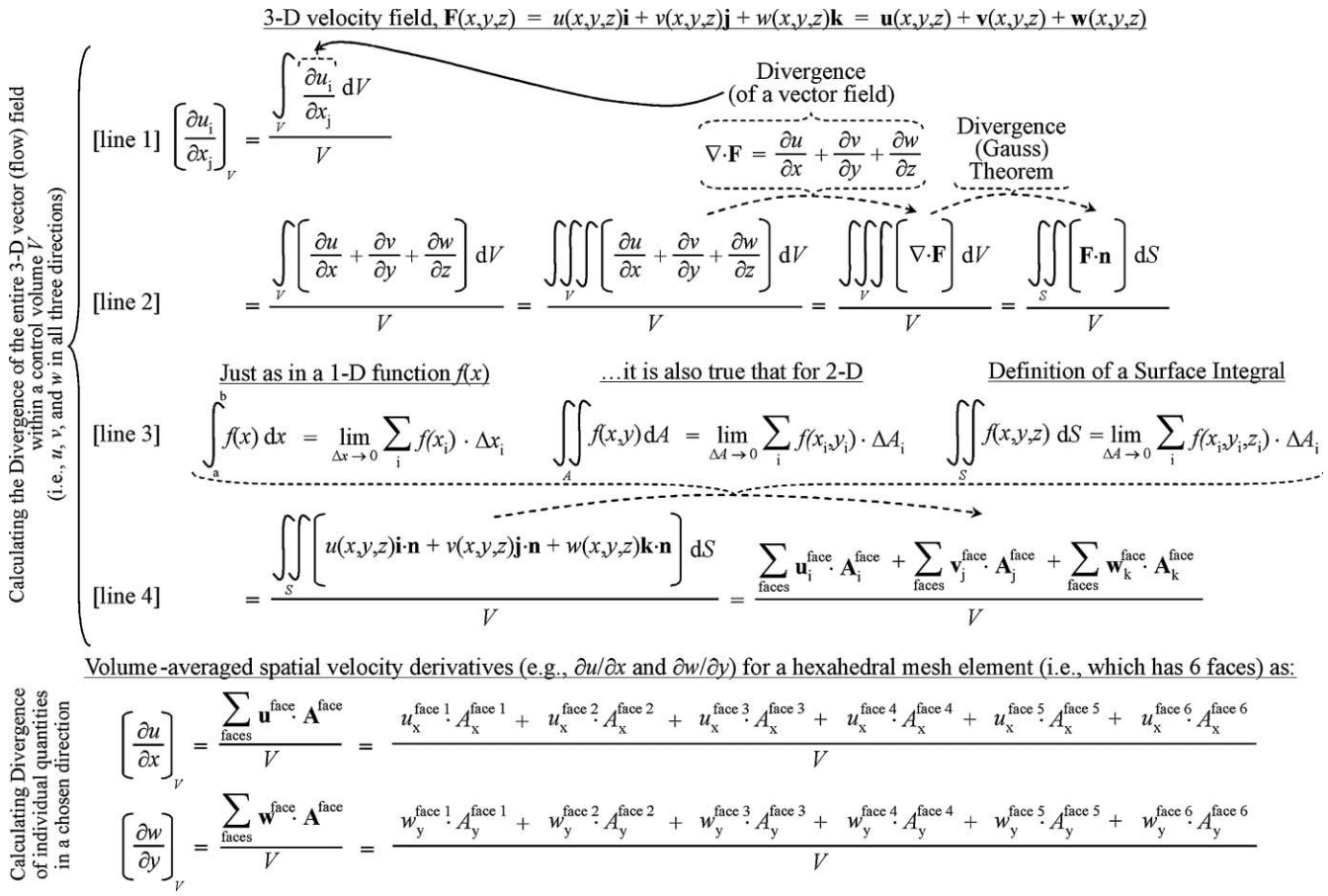
3-D velocity field, $\mathbf{F}(x,y,z) = u(x,y,z)\mathbf{i} + v(x,y,z)\mathbf{j} + w(x,y,z)\mathbf{k} = \mathbf{u}(x,y,z) + \mathbf{v}(x,y,z) + \mathbf{w}(x,y,z)$
Calculating the Divergence of the entire 3-D vector (flow) field within a control volume V (i.e., u, v, and w in all three directions)
[line 1] $\left[\frac{\partial u_i}{\partial x_j}\right]_V = \frac{\int_V \frac{\partial u_i}{\partial x_j}\,dV}{V}$
Divergence (of a vector field)
$\nabla\cdot\mathbf{F} = \frac{\partial u}{\partial x} + \frac{\partial v}{\partial y} + \frac{\partial w}{\partial z}$
Divergence (Gauss) Theorem
[line 2] $= \frac{\int_V \left[\frac{\partial u}{\partial x} + \frac{\partial v}{\partial y} + \frac{\partial w}{\partial z}\right] dV}{V} = \frac{\iiint_V \left[\frac{\partial u}{\partial x} + \frac{\partial v}{\partial y} + \frac{\partial w}{\partial z}\right] dV}{V} = \frac{\iiint_V \left[\nabla\cdot\mathbf{F}\right] dV}{V} = \frac{\iint_S \left[\mathbf{F}\cdot\mathbf{n}\right] dS}{V}$
Just as in a 1-D function $f(x)$
…it is also true that for 2-D
Definition of a Surface Integral
[line 3] $\int_a^b f(x)\,dx = \lim_{\Delta x\to 0}\sum_i f(x_i)\cdot\Delta x_i \qquad \iint_A f(x,y)\,dA = \lim_{\Delta A\to 0}\sum_i f(x_i,y_i)\cdot\Delta A_i \qquad \iint_S f(x,y,z)\,dS = \lim_{\Delta A\to 0}\sum_i f(x_i,y_i,z_i)\cdot\Delta A_i$
[line 4] $= \frac{\iint_S \left[u(x,y,z)\mathbf{i}\cdot\mathbf{n} + v(x,y,z)\mathbf{j}\cdot\mathbf{n} + w(x,y,z)\mathbf{k}\cdot\mathbf{n}\right] dS}{V} = \frac{\sum_{\text{faces}} \mathbf{u}_i^{\text{face}}\cdot\mathbf{A}_i^{\text{face}} + \sum_{\text{faces}} \mathbf{v}_j^{\text{face}}\cdot\mathbf{A}_j^{\text{face}} + \sum_{\text{faces}} \mathbf{w}_k^{\text{face}}\cdot\mathbf{A}_k^{\text{face}}}{V}$
Volume-averaged spatial velocity derivatives (e.g., $\partial u/\partial x$ and $\partial w/\partial y$) for a hexahedral mesh element (i.e., which has 6 faces) as:
Calculating Divergence of individual quantities in a chosen direction
$\left[\frac{\partial u}{\partial x}\right]_V = \frac{\sum_{\text{faces}} \mathbf{u}^{\text{face}}\cdot\mathbf{A}^{\text{face}}}{V} = \frac{u_x^{\text{face 1}}\cdot A_x^{\text{face 1}} + u_x^{\text{face 2}}\cdot A_x^{\text{face 2}} + u_x^{\text{face 3}}\cdot A_x^{\text{face 3}} + u_x^{\text{face 4}}\cdot A_x^{\text{face 4}} + u_x^{\text{face 5}}\cdot A_x^{\text{face 5}} + u_x^{\text{face 6}}\cdot A_x^{\text{face 6}}}{V}$
$\left[\frac{\partial w}{\partial y}\right]_V = \frac{\sum_{\text{faces}} \mathbf{w}^{\text{face}}\cdot\mathbf{A}^{\text{face}}}{V} = \frac{w_y^{\text{face 1}}\cdot A_y^{\text{face 1}} + w_y^{\text{face 2}}\cdot A_y^{\text{face 2}} + w_y^{\text{face 3}}\cdot A_y^{\text{face 3}} + w_y^{\text{face 4}}\cdot A_y^{\text{face 4}} + w_y^{\text{face 5}}\cdot A_y^{\text{face 5}} + w_y^{\text{face 6}}\cdot A_y^{\text{face 6}}}{V}$